NASA TECHNICAL MEMORANDUM

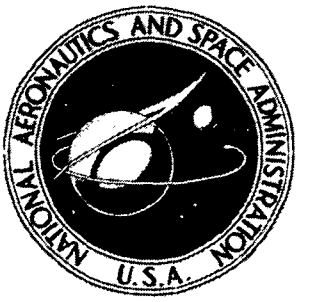

NASA TM X-2396

NASA TM X-2396

FLIGHT INVESTIGATION OF AIRFRAME INSTALLATION EFFECTS ON AN AUXILIARY INLET EJECTOR NOZZLE ON AN UNDERWING ENGINE NACELLE

by Richard R. Burley

Lewis Research Center
Cleveland, Ohio 44135

NATIONAL AERONAUTICS AND SPACE ADMINISTRATION • WASHINGTON, D. C. • NOVEMBER 1971

1. Report No.	2. Government Accession No.	3. Recipient's Catalog No.
NASA TM X-2396		

4. Title and Subtitle	5. Report Date
FLIGHT INVESTIGATION OF AIRFRAME INSTALLATION EFFECTS ON AN AUXILIARY INLET EJECTOR NOZZLE ON AN UNDERWING ENGINE NACELLE	November 1971
	6. Performing Organization Code

7. Author(s)	8. Performing Organization Report No.
Richard R. Burley	E-6208
	10. Work Unit No. 720-03

9. Performing Organization Name and Address	11. Contract or Grant No.
Lewis Research Center National Aeronautics and Space Administration Cleveland, Ohio 44135	

12. Sponsoring Agency Name and Address	13. Type of Report and Period Covered
National Aeronautics and Space Administration Washington, D.C. 20546	Technical Memorandum
	14. Sponsoring Agency Code

15. Supplementary Notes

16. Abstract

The local flow field approaching an installed nozzle may vary from isolated test conditions, thereby affecting exhaust nozzle performance. An installation of general interest is a podded engine mounted near the aft lower surface of the wing. The effect of this installation on the performance of an auxiliary inlet ejector nozzle was investigated over a Mach number range of 0.7 to 1.3 by using a modified F-106B aircraft. Both floating and fixed-open door configurations were examined. The ejector nozzle trailing-edge flaps were simulated in the closed position with rigid structure which provided a boattail angle of 15°. Primary nozzle area was varied as exhaust gas temperature was varied between 982.2 and 2003.3 K (1768° and 3606° R).

17. Key Words (Suggested by Author(s))	18. Distribution Statement
Airframe installation effects; Propulsion system; Transonic; Flight test; Auxiliary inlet ejector	Unclassified - unlimited

19. Security Classif. (of this report)	20. Security Classif. (of this page)	21. No. of Pages	22. Price*
Unclassified	Unclassified	71	$3.00

* For sale by the National Technical Information Service, Springfield, Virginia 22151

CONTENTS

FLIGHT INVESTIGATION OF AIRFRAME INSTALLATION EFFECTS ON AN AUXILIARY INLET EJECTOR NOZZLE ON AN UNDERWING ENGINE NACELLE

by Richard R. Burley

Lewis Research Center

SUMMARY

The local flow field approaching an installed nozzle may vary from isolated test conditions, thereby affecting nozzle performance. To determine the performance of an installed auxiliary inlet ejector nozzle, a flight investigation was conducted over a Mach number range of 0.7 to 1.3 and a comparison was made with the results obtained from a small-scale isolated model. The installation consisted of a podded engine mounted near the aft lower surface of the wing with the exhaust nozzle extending beyond the wing trailing edge. Both floating and fixed-open door configurations were tested at diameter ratios d_9/d_8 (ejector-exit diameter to primary-nozzle-exit effective diameter) of 1.55, 1.40, and 1.23. These diameter ratios correspond to primary nozzle power settings of military, minimum afterburner, and maximum afterburner, respectively. The ejector trailing-edge flaps were simulated in the closed position with rigid structure which provided a boattail angle of 15°. Primary jet exhaust was provided by a calibrated turbojet engine (J85-GE-13) and the secondary air was obtained from the nacelle inlet. Primary exhaust gas temperature varied between 982.2 and 2003.3 K (1768° and 3606° R). A corrected secondary weight flow ratio of 0.035 was used for d_9/d_8 values of 1.55 and 1.40; a corrected secondary weight flow ratio of 0.05 was used with $d_9/d_8 = 1.23$. The effect of weight flow ratio also was studied as was the effect of door blockage (as might occur due to the routing of electronic or hydraulic lines).

Comparison of results from the isolated and installed nozzles show that, at minimum afterburner power, there was an unfavorable installation effect for Mach numbers less than 0.9 and a favorable effect for Mach numbers between 0.9 and 1.0. At maximum afterburner power, there was a favorable installation effect for Mach numbers between 0.9 and 1.0 (no data were taken below $M_0 = 0.9$). For the installed nozzle, the doors floated to the position that gave close to optimum performance. This was not the case for the isolated nozzle, where the doors floated too far closed resulting in performance considerably below optimum. Results for the installed nozzle indicate that higher performance was obtained with the double-hinge fixed-open doors than with the single-hinge fixed-open doors.

INTRODUCTION

The local flow field approaching an installed nozzle may vary from isolated test conditions, thereby affecting nozzle performance (ref. 1). This is especially true in the transonic speed range where the nozzle is operating off design and external flow effects are important. The Lewis Research Center is currently investigating installation effects on supersonic cruise nozzles in the transonic speed range (refs. 2 to 4). One of the interesting nozzle types is the auxiliary inlet ejector nozzle. It has the potential for achieving the performance normally associated with more complex variable-geometry designs but at reduced weight (ref. 5). This is due to the principle of self actuation for both the auxiliary inlet doors and the trailing-edge flaps, which are positioned by the pressure differential across them. The variation in the local flow field can affect nozzle performance by changing the tertiary air inlet conditions and the external pressure drag. The doors may close prematurely or the trailing-edge flap may float to a larger exit area and thereby produce overexpansion losses. A variation in boundary layer height and profile can also affect the tertiary flow and consequently the internal performance.

The present investigation was conducted to determine the performance of an installed auxiliary inlet ejector nozzle over a Mach number range of 0.7 to 1.3 and to compare it with the results obtained from an isolated model. The results from the isolated model were obtained in the 8- by 6-Foot Supersonic Wind Tunnel with a 0.34-scaled cold-flow model (ref. 6). The installation consisted of a podded engine mounted near the aft lower surface of the wing with the exhaust nozzle extending beyond the wing trailing edge. This aft location of the nacelle provides shielding of the inlet by the forward wing surface to minimize angle-of-attack effects and may also provide favorable interference effects between the wing and nacelle flow fields. A wing cutout was provided so that the top three auxiliary inlet doors opened to the top of the wing. Both floating and fixed-open door configurations were tested at diameter ratios d_9/d_8 (ejector-exit diameter to primary-nozzle-exit effective diameter) of 1.55, 1.40, and 1.23. These diameter ratios correspond to military, minimum afterburner, and maximum afterburner power settings, respectively. The trailing-edge flaps were simulated in the closed position with rigid structure which provided a boattail angle of 15°. A static investigation of this nozzle has also been conducted (ref. 7). The primary jet exhaust was provided by a calibrated turbojet engine (J85-GE-13) and the secondary air was obtained from the nacelle inlet. The primary exhaust gas temperature varied between 982.2 and 2003.3 K (1768° and 3606° R). A corrected secondary weight flow ratio of 0.035 was used for d_9/d_8 values of 1.55 and 1.40; a weight flow ratio of 0.05 was used with $d_9/d_8 = 1.23$. The effect of changing the weight flow ratio was also studied as was the effect of door blockage (as might occur due to the routing of electronic or hydraulic lines).

APPARATUS AND PROCEDURE

Flight Installation

Flight tests were conducted with an F-106B aircraft modified to carry two underwing nacelles. The aircraft in flight is shown in figure 1 with the auxiliary inlet ejector nozzle installed on the left nacelle. A schematic view of the nacelle-engine installation is shown in figure 2. The 63.5-centimeter (25.0-in.) diameter nacelles were located at approximately 32 percent semispan with the exhaust nozzles extending beyond the wing trailing edge. Since the nozzles would interfere with normal elevon movement, a section of the elevon immediately above each nacelle was cut out and rigidly fixed to the wing. For the present tests, the rigid section on the left wing was modified in the form of a trough. Also, a wide nacelle strut that faired back into the elevon trough was used. Details of the nacelle strut are given in reference 4. The nacelle had a normal shock inlet and contained a calibrated J85-GE-13 afterburning turbojet engine. Secondary air to cool the engine and afterburner was supplied from the inlet and was controlled at the periphery of the compressor face by a calibrated rotary valve. The normal shock inlet faired into a bulged section on the bottom of the nacelle to accommodate the engine accessory package.

Each nacelle was attached to the wing by two links normal to the nacelle axis and the axial force was measured by a load cell attached to the wing. An accelerometer in the nacelle allowed the load cell to be compensated for axial acceleration. The axial force transmitted to the compensated load cell can be divided into two parts: (1) nacelle drag forward of the research nozzle, referred to as the tare force; and (2) research nozzle gross thrust minus drag. The tare force was determined during prior flights by using a calibrated cylindrical ejector nozzle (ref. 8). The research nozzle gross thrust minus drag was determined by subtracting the tare force from the compensated load-cell reading.

Primary Nozzle

The variable-area primary exhaust nozzle is made up of overlapping leaves that provide a nearly circular throat area. The leaves translate on a roller-track-cage arrangement, causing a change in the nozzle convergence angle (fig. 3).

Auxiliary Inlet Ejector

The ejector nozzle, along with the elevon trough and the auxiliary inlet doors, is shown in figure 4 and the details are presented in figures 5 and 6. The ejector nozzle incorporates a series of 16 auxiliary inlet doors located around the periphery of the external skin ahead of the primary nozzle, with the top three doors opened to the trough (fig. 4(a)). Details of the auxiliary inlet doors are shown in figures 5(a) to (c). The doors were either in fixed positions or allowed to float under the influence of air loads. The floating doors were double hinged with a 2-to-1 ratio between the aft and the forward ramp angles. The forward and aft door ramps were the same length. Each floating door had a variable friction device consisting of spring washers and a self-locking nut (fig. 5(c)). The doors were installed with the spring washers loose because the results of shake table tests indicated that the doors were less subject to vibration with no damping. The fixed doors consisted of three sets of double-hinge doors (5°-10°, 8°-16°, 10°-20°), two sets of single-hinge doors (16° and 20°), and closed doors. The doors positioned at 20° or 10°-20° (full open) resulted in an open area A_{AID} of 1052 square centimeters (163 in.^{2}); positioning the doors at 16° or 8°-16° resulted in A_{AID} of 883.2 square centimeters (136.9 in.^{2}); positioning the doors at 5°-10° resulted in A_{AID} of 576.8 square centimeters (89.4 in.^{2}).

The ejector trailing-edge flaps, which were simulated in the closed position with rigid structure, provided a boattail angle of 15° and an exit diameter of 46.2 centimeters (18.19 in.) as shown in figure 6(a). The boattail juncture radius was 0.5 nacelle diameters. The primary nozzle housing, also shown in figure 6(a), has a series of 24 rectangular holes located circumferentially around the ring. The holes were covered by a plate and the secondary flow deflector was positioned near the forward part of the housing so that the secondary cooling air went under the housing and over the primary nozzle. Detailed dimensions of the elevon trough are shown in figure 6(b).

The primary nozzle effective area A_8 was set at nominal values of 700, 858, and 1116 square centimeters (108, 133, and 173 in.^{2}), corresponding to military, minimum afterburning, and maximum afterburning power settings, respectively. The variation in diameter ratio d_S/d_8 and spacing ratios L_e/d_8 and L/d_8 with primary nozzle effective area are shown in figure 7.

The principal purpose of the doors is to allow outside air to enter the ejector and provide an aerodynamically smaller ejector exit area, which helps reduce the overexpansion of the primary jet at low values of nozzle pressure ratio. The difference between the actual ejector exit area and the ejector exit area required to properly expand the primary flow is referred to as the overexpansion area A_{OE}. The variation in overexpansion area with flight Mach number is presented in figure 7(b) for the three diameter ratios of principal interest. The ejector nozzle is overexpanded ($A_{OE} > 0$) over the entire range of Mach numbers and diameter ratios investigated.

Also shown in figure 7(b) are the auxiliary-inlet-door open areas A_{AID} for doors positioned at 5°-10°, 16° or 8°-16°, and 20° or 10°-20°. When the doors are positioned at 16° or 8°-16°, the open area is greater than the overexpansion area over the entire range of Mach numbers and diameter ratios tested.

Instrumentation

Total pressure and temperature of the secondary air were obtained from probes, as shown in figure 8. The probes were located beneath the primary nozzle housing at 0°, 90°, 180°, and 270°. The thermocouples were Chromel-Alumel and had radiation shields.

Instrumentation for the ejector nozzle and auxiliary inlet doors is presented in figure 9. Boundary-layer rakes were positioned just upstream and downstream of the auxiliary inlet doors at the four circumferential locations shown in figure 9(a). Also shown in figure 9(a) are the five tertiary total-pressure rakes. Each is located just downstream of an auxiliary inlet door. Each of these five doors has a row of equally spaced external static-pressure orifices located along the door centerline. The axial stations of these orifices are given in figure 9(b). The static pressure acting on the internal surface of the doors was obtained from orifices located on three internal struts of the ejector nozzle, as shown in figure 9(c). The floating doors were similarly instrumented and the position of each floating door was measured by a potentiometer. External static-pressure instrumentation on the ejector nozzle is shown in figure 9(d). Four rows of static-pressure orifices were located on the cylindrical portion of the nozzle upstream of the doors at 0°, 90°, 180°, and 315°. Three rows of static-pressure orifices were located on the cylindrical portion of the nozzle downstream of the doors and on the boattail at 0°, 90°, and 180°. Internal static-pressure and wall temperature instrumentation is shown in figure 9(e). Three rows of each were located at 0°, 90°, and 180°; an additional row of static-pressure orifices was located at 45°. A pressure tube was located in the cavity formed by the inner surface of the boattail and the gas-side surface of the nozzle. It was used in calculating the trailing-edge-flap moment. Skin temperatures were measured with the juncture of the Chromel-Alumel thermocouple embedded in the skin, flush with the hot surface side.

An onboard digital data system was used to record the pressure and temperatures on magnetic tape. It has the capability of recording 578 parameters in 11.6 seconds (ref. 8). The position of 14 of the 16 floating doors also was recorded on the digital system. The position of all 16 floating doors was recorded on the onboard analog system. This system records dynamic data on magnetic tape in frequency modulation (FM) form and has a capacity of 52 channels (ref. 8).

A flight-calibrated test boom located on the aircraft nose was used to determine free-stream static and total pressures, aircraft angle of attack, and sideslip angle.

Procedure

Performance characteristics of the ejector nozzle were obtained over flight Mach numbers from 0.7 to 1.3 and at Reynolds numbers that varied from 1.03×10^5 per centimeter (3.15×10^6/ft) at Mach 0.7 to 1.4×10^5 per centimeter (4.4×10^6/ft) at Mach 1.3. The aircraft was flown at the nominal altitude - Mach number profile shown in figure 10(a), which resulted in the angles of attack and trim elevon deflection shown in figure 10(b). The exhaust nozzle pressure ratio schedule is given in figure 10(c) as a function of Mach number. Seven door configurations and four power settings were investigated. The four power settings and the resulting nominal values of primary nozzle effective area A_8 and corresponding values of diameter ratio d_9/d_8, exhaust gas temperature T_8, and corrected secondary weight flow ratio $(\omega\sqrt{\tau})_s$ are given in table I; the seven door configurations are

(1) Floating doors

(2) Fixed-open doors

(a) Double hinge: 5^o-10^o, 8^o-16^o, 10^o-20^o

(b) Single hinge: 16^o, 20^o

(3) Closed doors

(The reheat A power setting was used only to study the effect of changing corrected secondary weight flow ratio.) Each door configuration was tested at military, minimum afterburner, and maximum afterburner power settings. In addition, the floating and 10^o-20^o fixed-open door configurations were investigated at reheat A power setting over a range of corrected secondary weight flow ratios from 0.030 to 0.055 at a Mach number of 0.9.

Data Reduction

Engine airflow was determined by using the calibration results from reference 9 along with measurements of engine speed and total pressure and temperature at the compressor face. Fuel flows were obtained from calibrated flowmeters. Total temperature T_8, total pressure P_8, and effective area A_8 were obtained by using the values of engine airflow and fuel flow, the measured values of total pressure and temperature at the turbine discharge, and afterburner temperature rise and pressure drop calibration results from reference 9.

The ejector nozzle gross thrust minus drag is defined as follows. Gross thrust is the total momentum of the internal flow at the ejector exit minus the total momentum of the tertiary air at the entrance to the auxiliary inlet doors. The drag is the sum of the pressure drop on the boattail and the skin friction drag. Skin-friction calculations were based on an equivalent wetted area of a flat plate and an average Reynolds number. Pressure drags were obtained by assigning to each pressure orifice an incremental area projected on a plane normal to the nozzle axis and summing the incremental forces. Tertiary airflow was calculated by using the free-stream total temperature and the static pressures measured on the shroud wall in the plane of the tertiary total-pressure rakes, and by assigning to each total-pressure tube an incremental flow area. In instances where a total pressure is less than its associated static, it was assumed that no flow went into or out of the incremental flow area.

Three different performance parameters are presented. The first, nozzle gross thrust coefficient, is defined as ejector nozzle actual gross thrust minus drag divided by the ideal thrust of the primary stream:

$$\frac{F - D}{F_{ip}}$$

The second performance parameter, nozzle performance coefficient, is identical to the first except that the ram drag of the secondary airflow is subtracted. This accounts for losses associated with bringing the secondary air on board:

$$\frac{F - D}{F_{ip}} - \frac{m_s V_0}{F_{ip}}$$

The third parameter, internal performance coefficient, excludes the external drag of the nozzle:

$$\frac{F - D}{F_{ip}} - \frac{C_{D,\beta} + C_{f,\beta} + C_{f,CS} + C_{D,AID} + C_{f,AID}}{F_{ip}} q_o A_n$$

The ideal thrust of the primary stream F_{ip} was calculated from the measured primary mass flow expanded isentropically from its value of total pressure and temperature to ambient pressure.

RESULTS AND DISCUSSION

This section is divided into three major subdivisions. The first compares the results of the installed nozzle and the isolated nozzle to determine the effect of the installation. This is done for both the floating and the fixed door configurations. The next two subdivisions present the results of the installed nozzle, first for the floating door configuration and then for the fixed door configurations.

Performance Comparison of Installed and Isolated Nozzles

As will be shown in the next subdivision, peak performance of the installed nozzle at minimum afterburner power and over the Mach number range of 0.7 to 0.95 occurs with the doors open to about the 8°-16° position; at maximum afterburner power and over the Mach number range of 0.9 to 1.3, it occurs with the doors closed. Peak performance for the isolated nozzle (ref. 6) at maximum afterburner power also occurs with the doors closed. But at minimum afterburner power, it occurs with the double-hinge doors full open (10°-20°).

A comparison of the peak performance of the installed nozzle with that of the isolated nozzle is shown in figures 11(a-1) and (a-2) as a function of Mach number. Figure 11(a-1) presents the results at minimum afterburner power and figure 11(a-2) shows them for maximum afterburner power. At minimum afterburner power, the performance of the installed nozzle was lower than that of the isolated nozzle for Mach numbers below 0.9. However, for Mach numbers between 0.9 and 1.0, the performance of the installed nozzle was higher than that of the isolated nozzle. At maximum afterburner power, the installed nozzle also gave higher performance than the isolated nozzle for Mach numbers between 0.9 and 1.0.

Figure 11(b) presents the comparison in terms of boattail pressure drag for both minimum (fig. 11(b-1)) and maximum (fig. 11(b-2)) afterburner power. Installation of the nozzle caused a significant reduction in boattail drag especially at high subsonic Mach numbers (0.9 to 0.95) as the terminal shock moved toward the boattail increasing the pressure on the boattail. Above Mach 0.95, the terminal shock moved aft of the boattail and the decreased pressure on the boattail resulted in an abrupt increase in drag.

Figure 12 shows, for both the installed and the isolated nozzle, how the nozzle gross thrust coefficient and the ratio of boattail pressure drag to ideal primary thrust are affected as the double-hinge doors are opened. The results are presented at minimum afterburner power for Mach numbers of 0.7, 0.8, 0.9, and 0.95. A large increase in performance occurred for both the installed and the isolated nozzle as the doors were opened to the 5°-10° position. The isolated nozzle performance continued

to increase as the doors were opened further and reached a maximum value with the doors full open. For the installed nozzle, however, performance peaked with the doors opened to about the 8°-16° position.

Also shown in figure 12 is the effect of double-hinge door position on the ratio of boattail pressure drag to ideal primary thrust. For both the isolated and the installed nozzle at low subsonic Mach numbers (0.7 and 0.8), a small decrease in boattail pressure drag occurred as the doors were opened. This was because the flow over the boattail recompressed to a slightly higher value with the doors open than with the doors closed. There is not much difference in boattail drag between the installed and the isolated nozzle at low subsonic Mach numbers. But at high subsonic Mach numbers (0.9 and 0.95), the drag of the installed nozzle is considerably lower than that of the isolated nozzle (as is also shown in fig. 11(b-1)). The difference in boattail pressure drag between the isolated and the installed nozzle accounts for the difference in nozzle gross thrust coefficient only when the doors are closed or partly open. With the doors full open, the internal performance of the installed nozzle apparently was considerably poorer than that of the isolated nozzle. Thus, the potential installation benefit available at high subsonic speeds, due to lower installed drag, is not realized with the doors full open.

Figure 13 shows how the nozzle gross thrust coefficient of the installed nozzle compares with that of the isolated nozzle for the single-hinge door configuration. The results are presented as a function of Mach number for minimum afterburner power. For both the 16° and the 20° door configurations (figs. 13(a) and (b), respectively), the performance of the installed nozzle was lower than that of the isolated nozzle for Mach numbers below about 0.85. Thus, at minimum afterburner power, an unfavorable installation effect occurred not only for the double-hinge doors but also for the single-hinge doors.

It has already been pointed out, in connection with figure 12, that the unfavorable installation effect at minimum afterburner power was apparently due to the relatively poor internal performance of the installed nozzle. Internal performance is affected by the external flow field ahead of the auxiliary inlet doors. In this region there is a considerable circumferential variation in boundary-layer height and profile (as previously reported (ref. 4)). This is illustrated in figure 14 for minimum afterburner power and the 8°-16° double-hinge doors. There is a region of relatively low energy within the boundary layer of the rake located near the top of the nozzle. It is especially evident at Mach 0.86 (fig. 14(c)). Also shown in figure 14 is the ratio of momentum thickness to nozzle maximum diameter for each of the three boundary-layer rakes. The momentum thickness ratio δ^{**}/d_n is greatest for the rake at 11°, which is near the top of the nozzle. The value for the isolated nozzle is also shown in figure 14 and is considerably less than the value near the top of the installed nozzle. On the inboard side and on the

bottom of the nozzle, however, the values for the installed nozzle are somewhat less than the value for the isolated nozzle.

One of the consequences of this adverse flow field is a lower total-pressure recovery inside the doors of the installed nozzle compared to that for the isolated nozzle. This is shown in figure 15 for minimum afterburner power and for 5°-10°, 8°-16°, and 10°-20° double-hinge doors. Also, it can be seen in figure 15 that the pressure recovery varied from door to door.

Figure 16 presents a comparison of the nozzle gross thrust coefficient for the installed and the isolated nozzle, each having floating doors. The results shown by the symbols are for minimum afterburner power and Mach numbers of 0.7, 0.8, 0.9, and 0.95. For the installed nozzle, the door position is the average position of the 16 doors since, as will be shown in the next subdivision, all the doors did not float to the same position. The curves are repeated from figure 12. For the installed nozzle, the doors floated to the position that gave close to peak performance obtained with the fixed doors. However, this was not the case for the isolated nozzle, where the doors floated too far closed and thus resulted in performance considerably below optimum.

Performance of Installed Nozzle With Floating Doors

For the installed nozzle, as just mentioned, the doors floated to the position that gave close to peak performance at minimum afterburner power. Figure 17 presents the comparison at military and maximum afterburner power. The results are shown as a function of Mach number. For both of these power settings, the doors also floated to the position that gave close to peak performance. Also shown in figure 17 is the average position of the floating doors. The doors floated to about the 7°-14° position at military power and almost closed, about 2°-4°, for maximum afterburner power.

The floating doors were pressure actuated and moved according to the pressure difference across them. The position of each of the 16 doors is shown in figure 18 for minimum afterburner power at a Mach number of 0.9. A considerable difference exists in the positions of the doors, which corresponds approximately to a circumferential gradient in local external static pressure. The relatively high external pressure region near the top of the nozzle is responsible for the doors being full open in the vicinity of the elevon trough. But the air drawn into the ejector through these doors was from a relatively low-energy region of the flow field. Near the bottom of the nozzle, as previously mentioned, a relatively high-energy region exists. But little of this higher energy air can get into the nozzle because the doors are almost completely closed. This situation contributes to the relatively poor performance of the installed nozzle.

During flight, the position of each of the 16 floating doors was recorded on the onboard analog system. A typical response of a floating door to changes in power setting

is illustrated in figure 19 for a Mach number of 0.9. From maximum afterburner power the throttle was pulled back, at a moderately fast rate, until military power was reached. The procedure was then reversed. The door exhibited stable operation. In-flight motion pictures of the floating doors showed that they remained stable over the entire range of flight conditions tested.

Although the auxiliary inlet doors were allowed to float, the trailing-edge flaps were not. They were simulated in the closed position with rigid structure. Figure 20 shows the direction the trailing-edge flaps would move if allowed to float. (The moment analysis is given in ref. 6.) At minimum afterburner power, the flaps would move off the inner stops at Mach 0.9 or less because the internal flow was effectively separated from the walls, resulting in high internal wall pressures relative to boattail pressures. As the Mach number increased above 0.9, the internal flow became effectively attached to the wall, lowering the internal flap pressure; and the external terminal shock around the nacelle increased the external boattail pressure. Consequently, the trailing-edge flaps would move toward the inner stops. At military power, the flaps would be on the inner stops only at Mach numbers very near 1.0. Isolated data of reference 10 indicate that this increased exit area would further reduce performance.

At maximum afterburner power, the flaps would be on the inner stops at Mach numbers from 0.98 to less than 0.9. The internal flow was effectively attached to the wall for some distance downstream of the secondary throat, providing low internal pressures relative to boattail pressures. As the Mach number increased, the nacelle terminal shock moved off the boattail and provided a sharp reduction in boattail pressures, which caused the tendency for the flaps to move off the inner stops.

Figure 21 illustrates how the nozzle gross thrust coefficient is affected by changing the corrected secondary weight flow ratio at Mach 0.9. The results are shown for power settings of military, minimum afterburning, and reheat A afterburning (d_9/d_8 = 1.55, 1.40, and 1.27, respectively). For all three power settings, the increase in nozzle gross thrust coefficient was nearly directly proportional to the increase in corrected secondary weight flow ratio. When the data were presented in terms of the nozzle performance coefficient, which accounts for the ram drag of the secondary airflow, there was not much change in performance as corrected secondary weight flow ratio was increased. Also shown in figure 21 is the effect of corrected secondary weight flow ratio on the average position of the floating doors. The doors exhibited a slight tendency to move to a more closed position as corrected secondary weight flow ratio was increased.

The principal purpose of the auxiliary inlet doors is to allow tertiary air to enter the nozzle and help reduce the overexpansion of the primary jet. As Mach number increases, the nozzle becomes less overexpanded and, consequently, less tertiary air is required. An estimate (using total-pressure rakes) of the amount of tertiary air entering the nozzle as a function of Mach number is presented in figure 22. Tertiary airflow is expressed in terms of a corrected tertiary weight flow ratio and the results are

presented for power settings of military and minimum afterburning. The amount of tertiary airflow entering the nozzle decreases quite sharply as the Mach number is increased above 0.8. This is especially evident at minimum afterburner power. Also shown in the figure is the effect of increasing corrected secondary weight flow ratio on corrected tertiary weight flow ratio at Mach 0.9. The results are presented for three power settings. As expected, the amount of tertiary air entering the nozzle decreases as more secondary air is supplied. But the decrease is rather small. For example, at military power, the corrected tertiary weight flow ratio decreased from about 0.16 to 0.15 as the corrected secondary weight flow ratio increased from 0.03 to 0.06.

Considerations such as the routing of electronic or hydraulic lines might dictate that some of the floating doors be blocked closed. Three door blockage configurations were investigated at minimum afterburner power and are shown in figure 23. In one configuration the top three doors were closed and in another the door under each elevon-nacelle juncture and the bottom door were blocked close. (Fig. 4(c) shows the doors under the outboard elevon-nacelle junction blocked closed.) These configurations resulted in about 19 percent of the door open area being blocked closed. In the third configuration two doors under each of the elevon-nacelle junctions and three doors at the bottom of the nozzle were closed. It resulted in about 44 percent of the door open area being blocked closed. For all three configurations the unblocked doors were allowed to float under the influence of air loads.

The effect of door blockage on nozzle gross thrust coefficient is shown in figure 23 for Mach numbers 0.7 and 0.9. Blocking closed as many as seven of the 16 doors did not have a marked effect on performance. Apparently sufficient tertiary airflow was provided through the remainder of the doors.

Performance of Installed Nozzle With Fixed Doors

A comparison of nozzle gross thrust coefficient at minimum afterburner power between double- and single-hinge fixed door configurations is shown in figures 24(a) and (b) as a function of Mach number. Figure 24(a) presents the comparison between 16° and 8°-16° doors and figure 24(b) shows it for the 20° and 10°-20° doors. (The 16° or 8°-16° door configurations provide an open area at the door trailing edge A_{AID} of 883.2 cm^2 (136.9 $in.^2$): for the 20° or 10°-20° door configurations, A_{AID} = 1052 cm^2 (163 $in.^2$)). The nozzle gross thrust coefficient was higher with the double-hinge doors than with the single-hinge doors. For the 8°-16° doors and at Mach 0.9, for example, the nozzle gross thrust coefficient was about 0.945, which is about 2 percent greater than that for the 16° doors.

Nozzle performance is also compared in terms of an internal performance coefficient which excludes the external drag of the nozzle. (External drag is the sum of the

pressure drag on the boattail and on the external surface of the doors plus skin friction.) There is no noticeable difference in the internal performance coefficient between the single- and double-hinge door configurations. This suggests that the major reason for the higher performance of the double-hinge door configurations is the lower pressure drag on the double-hinge doors. The effect of going from single-hinge to double-hinge doors on door drag is similar to the effect of rounding the boattail junction on boattail drag (ref. 2).

Another parameter that is indicative of a change in internal performance is the secondary-to-primary total-pressure ratio. A change in this parameter reflects a change in pressure level in the primary nozzle base region which, in turn, affects internal performance. A comparison of this parameter at minimum afterburner power between single- and double-hinge fixed door configurations is shown in figures 25(a) and (b) as a function of Mach number. Figure 25(a) presents the comparison between the 16° and 8°-16° doors and figure 25(b) shows it for the 20° and 10°-20° doors. Going from 16° to 8°-16° doors does not affect the value of secondary-to-primary total-pressure ratio. This is consistent with the previous result that there is no noticeable difference in internal performance when using either the 16° or the 8°-16° doors. However, going from 20° to 10°-20° doors does result in a slight increase in the value of secondary-to-primary total-pressure ratio. Thus it appears that at least some of the increase in the value of thrust minus drag with the 10°-20° doors as compared to the 20° doors comes from an increase in internal performance.

As previously mentioned, the 8°-16° doors gave close to optimum performance for military and minimum afterburner power. This was due principally to the increase in internal performance as tertiary air was drawn into the ejector. It can also be illustrated by examining the secondary-to-primary total-pressure ratio. An increase in secondary-to-primary total-pressure ratio for a constant value of corrected secondary airflow is the result of tertiary air entering the ejector nozzle. As the doors open and tertiary air enters the nozzle, additional air must be pumped by the nozzle, requiring an increased secondary total pressure. This, in turn, improves nozzle performance. Conversely, if the doors open and air escapes from the nozzle, the secondary total pressure decreases and so does nozzle performance.

Figure 26 presents the secondary-to-primary total-pressure ratio as a function of door opening for a Mach number of 0.9. The results are shown for both minimum and maximum afterburner power. At minimum afterburner power, the secondary total pressure continues to rise as the doors are opened until the 8°-16° door position is reached. Opening the doors wider has no noticeable effect on secondary total pressure. At maximum afterburner power, the secondary total pressure decreases as the doors open. Note that for both power settings, the door position that gives the highest value of secondary total pressure also gives close to peak nozzle performance. (See figs. 16 and 17 for door positions that give peak performance.)

Another indication of the effect of tertiary air entering the ejector is the static-pressure distribution along the internal surface of the nozzle. This is shown in figure 27 for minimum afterburner power and a Mach number of 0.9. With the doors closed (fig. 27(a)), the shroud static-pressure ratios p_w/P_8 are considerably below ambient pressure ratios p_0/P_8 throughout most of the nozzle. As the doors are opened to the 5^o-10^o position (fig. 27(b)), tertiary air enters the nozzle and increases the level of the wall static pressures although some overexpansion still occurs. As the doors are further opened to the 8^o-16^o position (fig. 27(c)), the wall static-pressure level increases and becomes essentially ambient or slightly above ambient throughout the nozzle. This suggests that more tertiary air enters the nozzle. Opening the doors to the wide-open position (fig. 27(d)) has little additional effect on internal pressures, suggesting that little, if any, additional tertiary air enters the nozzle.

Also, as mentioned, the closed doors gave highest performance at maximum afterburner power and the decrease in performance as the doors were opened was probably caused by air going out the doors. The static-pressure distribution along the internal surface of the nozzle is shown in figure 28 for maximum afterburner power and a Mach number of 0.9. With the doors closed (fig. 28(a)), the wall static pressures on the convergent surface ($x/d_8 < 0.5$) are slightly above ambient but the wall static pressures downstream of this surface are mostly below ambient. Opening the doors (figs. 28(b) to (d)) had no significant effect on the static-pressure distribution downstream of the convergent surface, suggesting that no appreciable tertiary air enters the ejector. However, opening the doors did affect the wall pressure distribution on the convergent surface, causing the downstream pressures ($0.25 < x/d_8 < 0.5$) to be higher than the upstream pressures. The difference became more pronounced as the doors were opened wider. This suggests that air was escaping from the nozzle through the doors.

The effect of corrected secondary weight flow ratio on nozzle performance is presented in figure 29 for the 10^o-20^o fixed door configuration. The results are shown at a Mach number of 0.9 and for power settings of military, minimum afterburning, and reheat A afterburning (d_9/d_8 = 1.55, 1.40, and 1.27, respectively). Increasing corrected secondary weight flow ratio from 0.035 to 0.060 increases nozzle gross thrust coefficient only about 1 percent. If the nozzle gross thrust coefficient is penalized for ram drag of the secondary airflow, there is no noticeable improvement in performance as corrected secondary weight flow ratio is increased.

SUMMARY OF RESULTS

An investigation was conducted to determine the performance of an installed auxiliary inlet ejector nozzle over a Mach number range of 0.7 to 1.3 and to compare it with the results obtained from an isolated nozzle. The ejector trailing-edge flaps were

simulated in the closed position with a rigid structure which provided a boattail angle of 15°. Both floating and fixed door configurations were investigated. The floating configuration consisted of double-hinge doors. The fixed door configurations consisted of three sets of double-hinge doors (5°-10°, 8°-16°, and 10°-20°), two sets of single-hinge doors (16° and 20°), and closed doors. Data were obtained over a range of corrected secondary weight flow ratios from 0.035 to 0.060, ejector-exit to primary-nozzle-exit effective diameter ratios d_9/d_8 of 1.55, 1.40, and 1.23, which correspond to military, minimum afterburner, and maximum afterburner power settings, respectively, of the primary nozzle. Primary exhaust gas temperatures ranged between 982.2 and 2003.3 K (1768° and 3606° R). Results of the investigation may be summarized as follows:

1. At minimum afterburner power, there was an unfavorable installation effect for Mach numbers less than 0.9 and a favorable effect for Mach numbers between 0.9 and 1.0. At maximum afterburner power, a favorable installation effect also occurred for Mach numbers from below 0.9 to 1.0.

2. The installation caused a favorable reduction in boattail pressure drag at subsonic Mach numbers. This effect tended to be offset, however, by relatively poor internal performance of the installed nozzle due to poor auxiliary inlet performance. This, in turn, resulted from large circumferential variations in static pressure which caused unsymmetrical door deflection and a distorted boundary layer upstream of the doors.

3. For the installed nozzle, the doors floated to about the same intermediate position as was estimated for the isolated nozzle. This position corresponded to near-optimum performance for the installed nozzle but considerably less than optimum performance for the isolated nozzle. Performance of the isolated nozzle could be significantly improved with the doors held full open.

4. Blocking closed seven of the 16 floating doors did not have a marked effect on performance.

5. Higher performance was obtained with double-hinge than with single-hinge fixed-open door configurations due principally to the lower external pressure drag on the double-hinge doors.

6. Increasing secondary corrected weight flow ratio from 0.035 to 0.060 at Mach 0.9 increased performance about $2\frac{1}{2}$ percent with the floating doors but only about 1 percent with the 10°-20° fixed-open doors.

7. If the trailing-edge flaps had been floating rather than fixed, they would have moved off the inner stop at a Mach number of 0.9 and less for minimum afterburner

power. At maximum afterburner power, the flaps would be on the inner stops at Mach numbers from less than 0.9 up to 0.98.

Lewis Research Center,
National Aeronautics and Space Administration,
Cleveland, Ohio, July 19, 1971,
720-03.

APPENDIX A

SYMBOLS

A	area (cold), cm^2 ($in.^2$)
A_{AID}	auxiliary-inlet-door open area, cm^2 ($in.^2$)
A_n	nozzle maximum cross-sectional area, 3166.9 cm^2 (490.9 $in.^2$)
A_{OE}	overexpansion area, cm^2 ($in.^2$)
A_8	primary-nozzle-exit effective flow area, cm^2 ($in.^2$)
B	axial length (fig. 5), cm (in.)
C_D	pressure drag coefficient, pressure drag/$q_o A_n$
C_f	external skin-friction drag coefficient, skin friction/$q_o A_n$
C_{MAID}	auxiliary-inlet-door opening moment coefficient, moment/$q_o A_n d_n$
C_{MTEF}	trailing-edge-flap opening moment coefficient, moment/$q_o A_n d_n$
D	nozzle drag, kN (lbf)
d_n	nozzle maximum diameter, 63.5 cm (25 in.)
d_S	ejector minimum shroud diameter, cm (in.)
d_8	primary-nozzle-exit effective diameter, cm (in.)
d_9	ejector-exit diameter, cm (in.)
F	nozzle thrust, kN (lbf)
h	pressure altitude, m (ft)
L	axial distance from primary nozzle exit to secondary throat, cm (in.)
Ld_8	axial location of primary nozzle throat, cm (in.)
L_e	axial distance from primary nozzle exit to ejector exit, cm (in.)
l	auxiliary-inlet-door length (fig. 5), cm (in.)
M	Mach number
δ^{**}/d_n	ratio of boundary-layer momentum thickness to nozzle maximum diameter
$m_s V_0$	ram drag of secondary airflow, kN (lbf)
P	absolute total pressure, kN/m^2 (psi)
p	absolute static pressure, kN/m^2 (psi)
q	dynamic pressure

R	maximum axial length of auxiliary inlet door section (see fig. 5), cm (in.)
r_β	boattail junction radius, cm (in.)
S	auxiliary-inlet-door dimension (see fig. 5), cm (in.)
T	absolute total temperature, K (^{o}R)
V/V_L	ratio of local to local-free-stream velocity
V_L/V_0	ratio of local-free-stream to free-stream velocity
W	weight flow, kg/sec (lbm/sec)
x	axial distance from primary nozzle exit, cm (in.)
Y	distance from nozzle external surface, cm (in.)
z	distance from flap internal surface, cm (in.)
α	aircraft angle of attack, deg
γ	primary nozzle convergence angle (fig. 3), deg
δ_e	elevon deflection angle (+down, -up), deg
ν	auxiliary inlet door angle (fig. 5), deg
ξ	moment-center for floating door moment analysis (fig. 51)
$(\omega\sqrt{\tau})_s$	corrected secondary weight flow ratio, $(W_s/W_8)\sqrt{T_s/T_8}$
$(\omega\sqrt{\tau})_t$	corrected tertiary weight flow ratio, $(W_t/W_8)\sqrt{T_0/T_8}$
φ	angle for floating door moment analysis (fig. 51)
ψ	moment-center for floating door moment analysis (fig. 51)

Subscripts:

AID	auxiliary inlet door
CS	cylindrical shroud
c	cavity
d	downstream
ip	one-dimensional isentropic expansion of primary flow
s	secondary
t	tertiary
u	upstream
w	ejector wall
β	boattail

0 free stream

8 nozzle throat

9 ejector exit

APPENDIX B

NOZZLE PERFORMANCE CHARACTERISTICS

Nozzle gross thrust coefficient, internal performance coefficient, and pumping characteristics are presented for each door configuration and for power settings of military, minimum afterburning, and maximum afterburning (d_9/d_8 values of 1.55, 1.40, and 1.23, respectively). Also shown are the ratio of nozzle pressure drag to ideal thrust ratio and the trailing-edge-flap moment coefficient. These results are presented in figures 30 to 50.

APPENDIX C

FLOATING-DOOR MOMENT ANALYSIS

The auxiliary inlet ejector nozzle results of reference 6 used fixed door configurations but included an estimate of nozzle performance based on assuming the doors could float. The method used to predict the equilibrium position of the doors is given here along with an indication of how well the method works.

A schematic view of a floating door and the forces acting on it is shown in figure 51. To determine the total hinge moment at ξ, the aft door ramp is considered to be a free body in equilibrium. Then the sum of the forces and moments about ψ are zero.

$$F_1 l_1 - F_2 l_2 = 0 \tag{C1}$$

$$F_1 \sin \nu_d - F_2 \sin \varphi_2 - F_3 \sin \varphi_3 = 0 \tag{C2}$$

$$F_1 \cos \nu_d + F_2 \cos \varphi_2 - F_3 \cos \varphi_3 = 0 \tag{C3}$$

The values of ν_2, φ_2, and l_2 are known for any particular door setting; F_1 and l_1 are determined from the measured pressure distribution on the aft door ramp; F_2, F_3, and φ_3 are determined from the solution of equation (C1) and the simultaneous solution of equations (C_2) and (C_3).

$$F_2 = F_1 \frac{l_1}{l_2} \tag{C4}$$

$$\varphi_3 = \tan^{-1} \frac{F_1 \sin \nu_d - F_2 \sin \varphi_2}{F_1 \cos \nu_d + F_2 \cos \varphi_2} \tag{C5}$$

$$F_3 = \frac{F_1 \sin \nu_d - F_2 \sin \varphi_2}{\sin \varphi_3} \tag{C6}$$

Then the moment about ξ caused by the forces on the aft door ramp is

$$m_{F\text{-}R} = F_3 l_3 = F_3 l_4 \cos(\nu_u - \varphi_3) \tag{C7}$$

where ν_u and l_4 are known for any particular door setting and φ_3 and F_3 are given by equations (C5) and (C6), respectively. The moment about ξ is then

$$m_\xi = m_{F\text{-}R} + F_5 l_5 \tag{C8}$$

A positive moment would cause the doors to move to a more open position; a negative moment would cause the doors to move to a more closed position.

The moment has been calculated for floating doors 1, 2, 3, 5, and 9 (see fig. 23 for circumferential location of the doors). The results, expressed in terms of a moment coefficient, are shown in figure 52 along with the position to which the doors floated. The results are presented as a function of Mach number for minimum afterburner power.

Since a door will, in general, float to its equilibrium position, the moment coefficient should be zero. (This is not true for a door that is forced against a stop.) The moment coefficient for doors 1 and 2 is zero for Mach numbers of 0.95 and greater. At lower Mach numbers where the doors are wide open, the moment coefficient is a positive value, indicating that the doors would open even wider if they were not against the stop. Thus, for these two doors, the moment calculation gives accurate results.

For the other three doors, the moment coefficient is close to zero for Mach numbers between 0.7 and 1.05. But at higher Mach numbers, the moment coefficient is a negative value increasing in magnitude with increasing Mach number. A possible explanation for this could be an inaccurate door position indicator. If the door was forced completely closed, the moment coefficient would be a negative value even though the indicator might show the door to be partly open.

Another reason concerns possible static-pressure gradients in the vicinity of the door. If significant gradients exist, the static pressure assumed to act on the internal and/or external surfaces of the door may not be representative of the true static pressure. Since there was very limited internal static-pressure instrumentation (fig. 9(c)), significant circumferential and longitudinal gradients could not be detected. However, a previous investigation (ref. 7), in which fairly extensive internal instrumentation was used, did not reveal any significant gradients. External static-pressure orifices were located along the door centerline so that longitudinal pressure gradients could be accounted for. But pressure gradients across the width of the door could not be detected. Since a circumferential static-pressure gradient exists around the external surface of the nozzle in the vincinity of the doors, it seems reasonable that a gradient might exist across the width of some of the doors.

REFERENCES

1. Nichols, Mark R.: Aerodynamics of Airframe - Engine Integration of Supersonic Aircraft. NASA TN D-3390, 1966.

2. Wilcox, Fred A.; Samanich, Nick E.; and Blaha, Bernard J.: Flight and Wind Tunnel Investigation of Installation Effects on Supersonic Cruise Exhaust Nozzles at Transonic Speeds. Paper 69-427, AIAA, June 1969.

3. Crabs, Clifford C.; Mikkelson, Daniel C.; and Boyer, Earle O.: An Inflight Investigation of Airframe Effects on Propulsion System Performance at Transonic Speeds. Presented at the 13th Annual Symposium of the Society of Experimental Test Pilots, Los Angeles, Calif., Sept. 25-27, 1969.

4. Mikkelson, Daniel C.; and Head, Verlon L.: Flight Investigation of Airframe Installation Effects on a Variable Flap Ejector Nozzle of an Underwing Engine Nacelle at Mach Numbers From 0.5 to 1.3. NASA TM X-2010, 1970.

5. Migdal, David; and Horgan, John J.: Thrust Nozzles for Supersonic Transport Aircraft. J. Eng. Power, vol. 86, no. 2, Apr. 1964, pp. 97-104.

6. Johns, Albert J.; and Steffen, Fred W.: Performance of an Auxiliary Inlet Ejector Nozzle with Fixed Inlet Doors and Triple-Hinge Trailing-Edge Flap. NASA TM X-2034, 1970.

7. Burley, Richard R.; and Mansour, Ali H.: Static Performance of an Auxiliary Inlet Ejector Nozzle Using an Afterburning Turbojet Gas Generator. NASA TM X-1999, 1970.

8. Groth, Harold W.; Samanich, Nick E.; and Blumenthal, Philip Z.: Inflight Thrust Measuring System For Under-Wing Nacelles Installed on a Modified F-106 Aircraft. NASA TM X-2356, 1971.

9. Antl, Robert J.; and Burley, Richard R.: Steady-State Airflow and Afterburning Performance Characteristics of Four J85-GE-13 Turbojet Engines. NASA TM X-1742, 1969.

10. Bresnahan, Donald L.: Performance of an Aerodynamically Positioned Auxiliary Inlet Ejector Nozzle at Mach Numbers from 0 to 2.0. NASA TM X-2023, 1970.

TABLE I. - ENGINE POWER SETTINGS

J85 power setting	Nozzle throat area, A_8		Ejector-exit diameter to primary-nozzle-exit effective diameter, d_9 d_8	Nozzle throat temperature, T_8		Corrected secondary weight flow ratio, $(\omega\sqrt{\tau})_s$
	cm	in.		K	^{o}R	
Military	700	108	1.55	982	1768	0.035
Minimum afterburning	858	133	1.40	1400	2520	.035
Reheat A	1039	166	1.27	1855	3339	0.03 to 0.055
Maximum afterburning	1116	173	1.23	2003	3606	.05

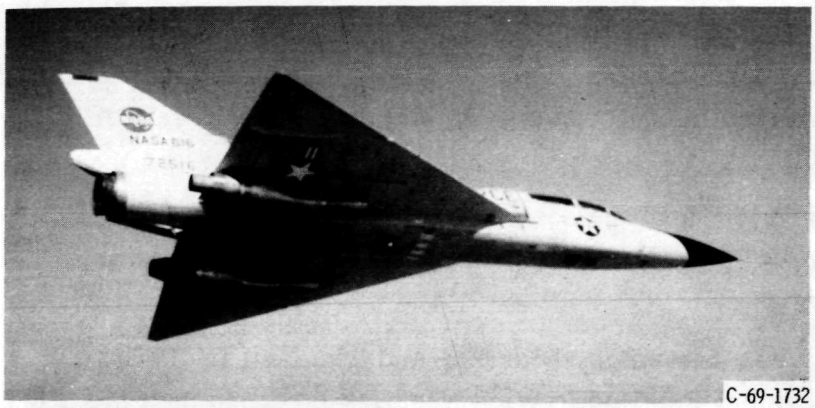

Figure 1. - Modified F-106B aircraft in flight.

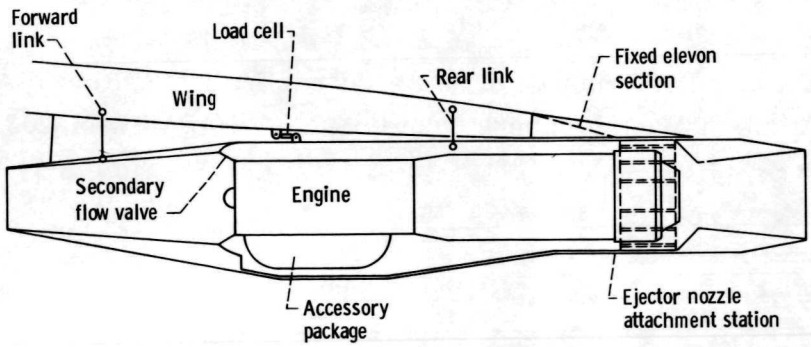

Figure 2. - Nacelle - engine installation.

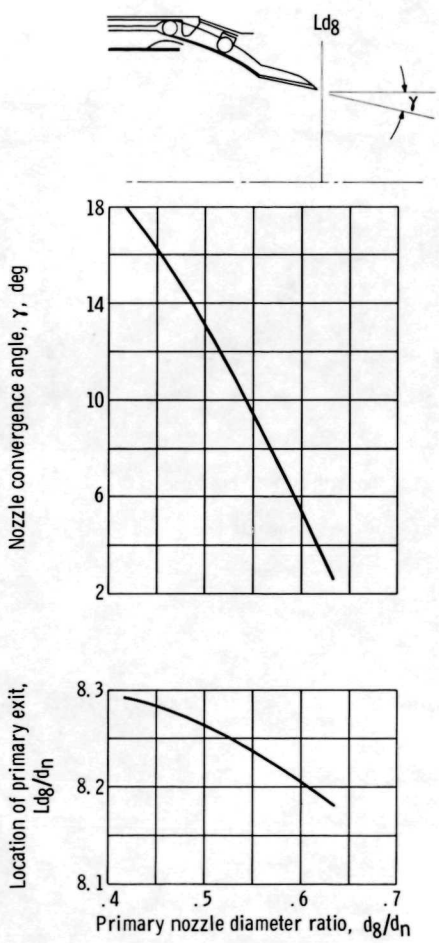

Figure 3. - Primary nozzle dimensional characteristics.

(a) With 10°-20° open doors.

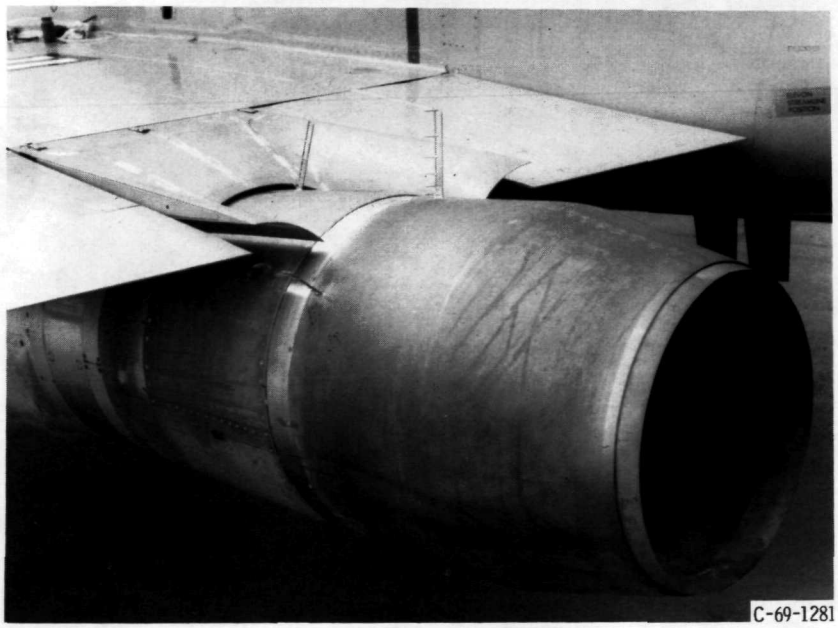

(b) With closed doors.

Figure 4. - Auxiliary inlet ejector nozzle.

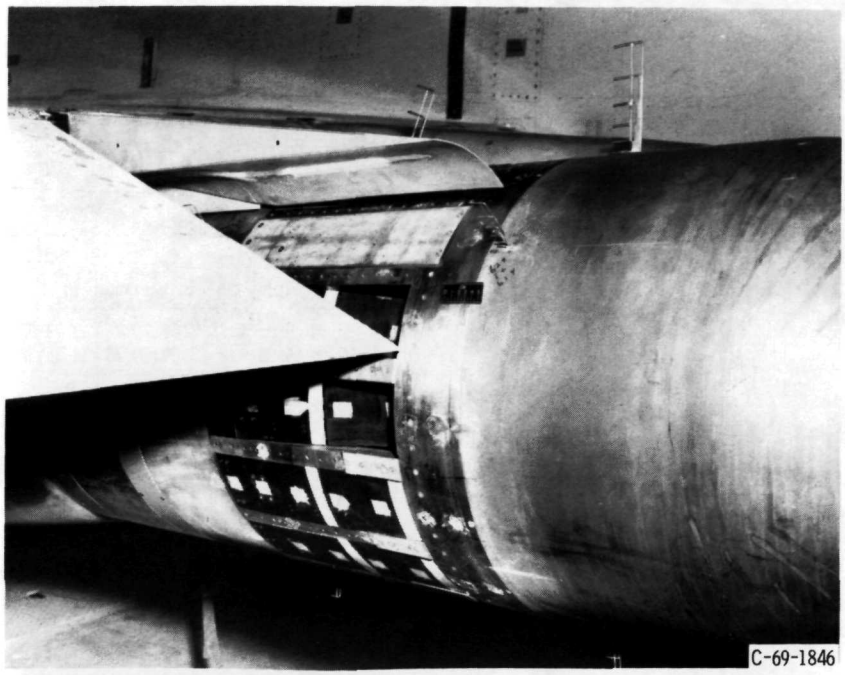

(c) Floating doors (with door blocked closed).

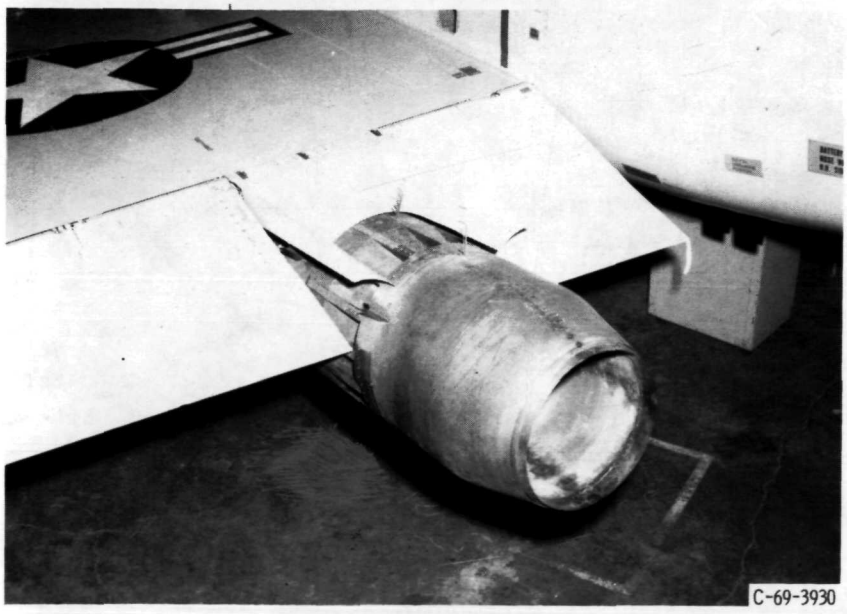

(d) With 20° open doors.

Figure 4. - Concluded.

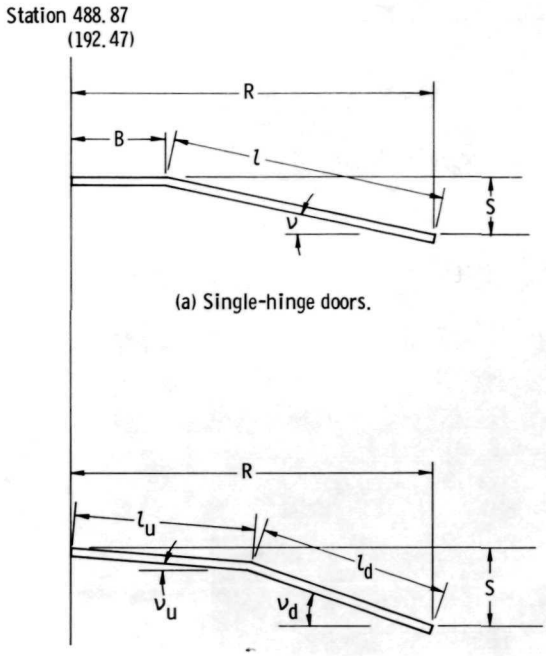

(a) Single-hinge doors.

ν, deg	l		S		R		B		A_{AID}	
	cm	in.	cm	in.	cm	in.	cm	in.	cm^2	$in.^2$
16	22.94	9.03	6.32	2.49	29.74	11.71	7.70	3.03	883.2	136.9
20	22.98	9.05	7.85	3.09	29.34	11.55	7.74	3.05	1052	163

ν_u, deg	ν_d, deg	l_u, l_d		S		R		A_{AID}	
		cm	in.	cm	in.	cm	in.	cm^2	$in.^2$
5	10	15.24	6	3.99	1.57	30.07	11.84	576.8	89.4
8	16	15.24	6	6.32	2.49	29.74	11.71	883.2	136.9
10	20	15.24	6	7.85	3.09	29.34	11.55	1052	163

(b) Double-hinge doors.

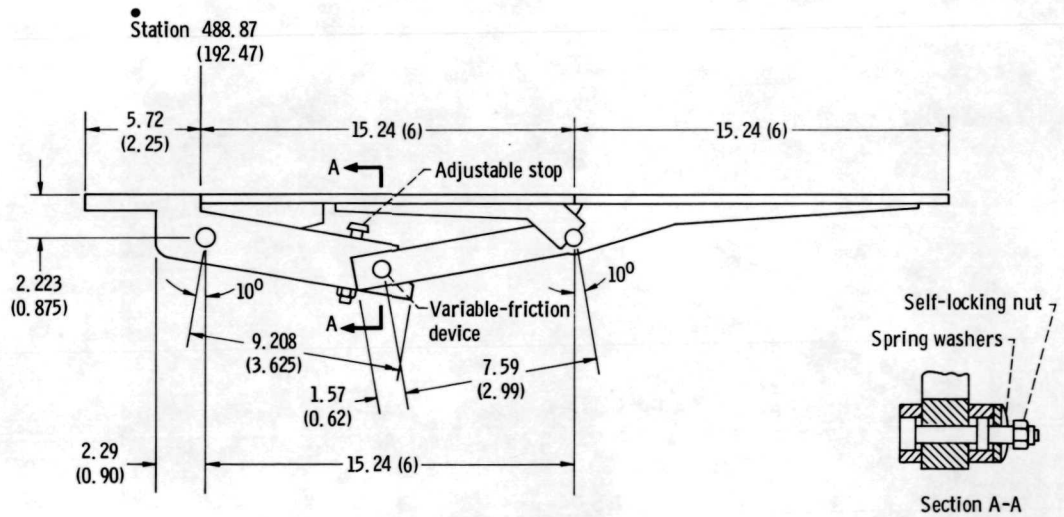

(c) Floating doors.

Figure 5. - Dimensional characteristics of auxiliary inlet doors. Door width, 9.83 centimeters (3.87 in.).

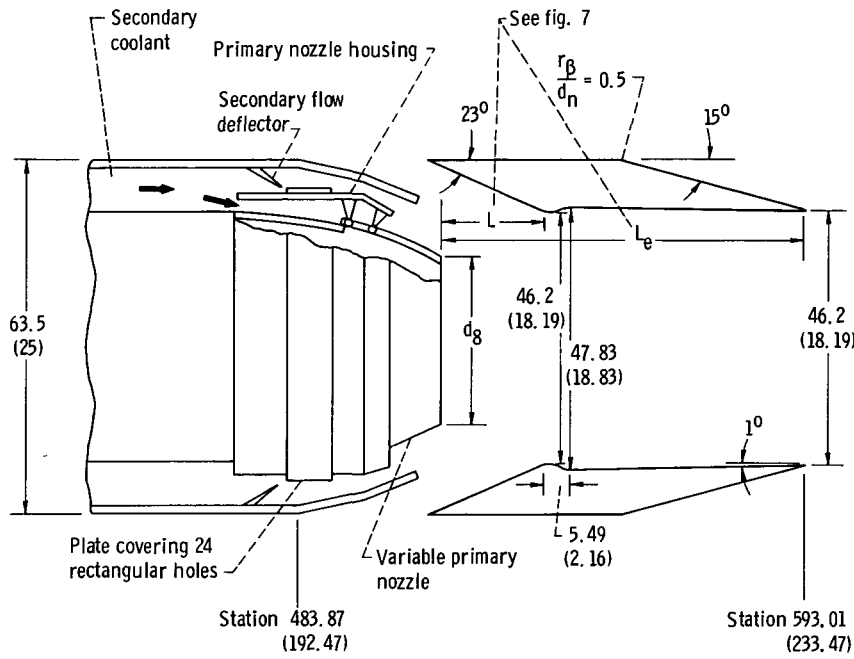

(a) Ejector nozzle.

Figure 6. - Dimensional characteristics of ejector nozzle and elevon trough. (All dimensions are in cm (in.).)

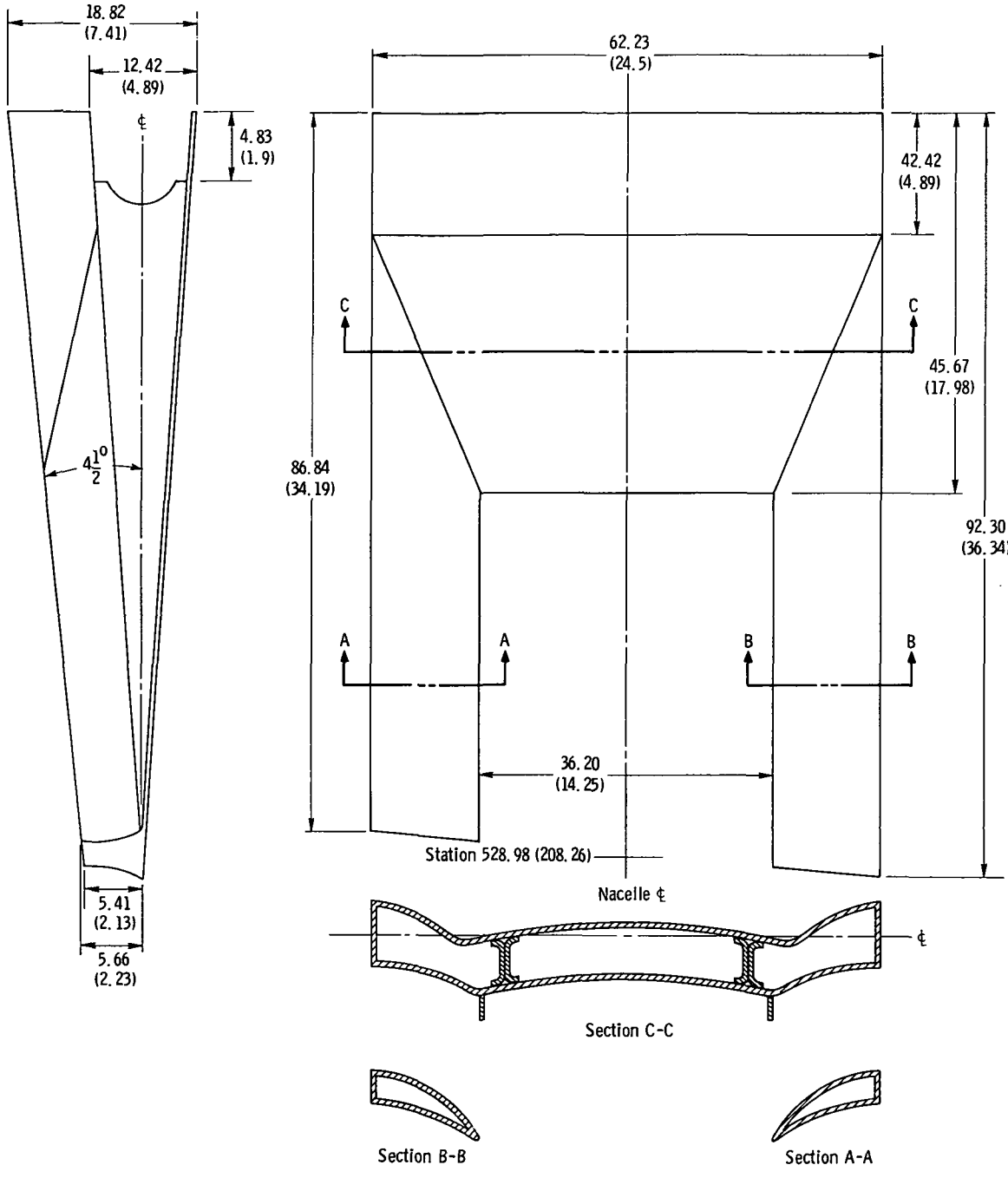

(b) Elevon trough.

Figure 6. - Concluded.

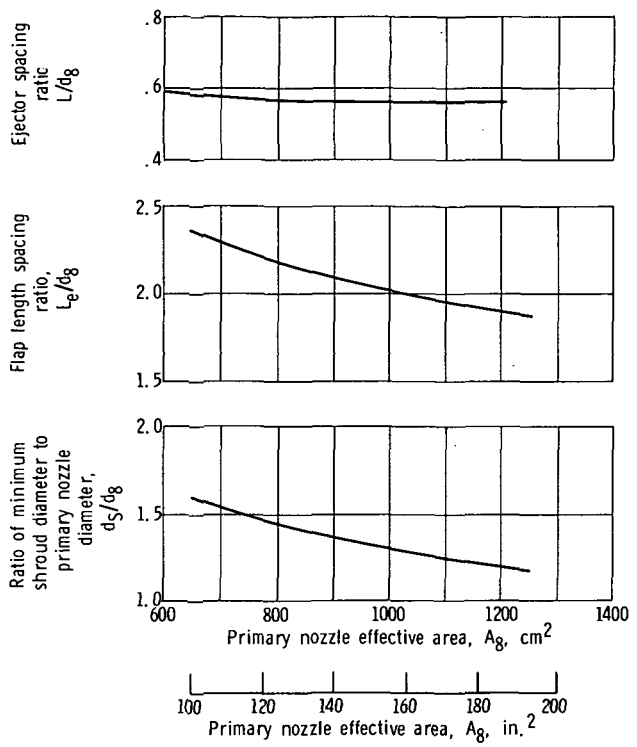

(a) Ejector diameter and spacing ratios.

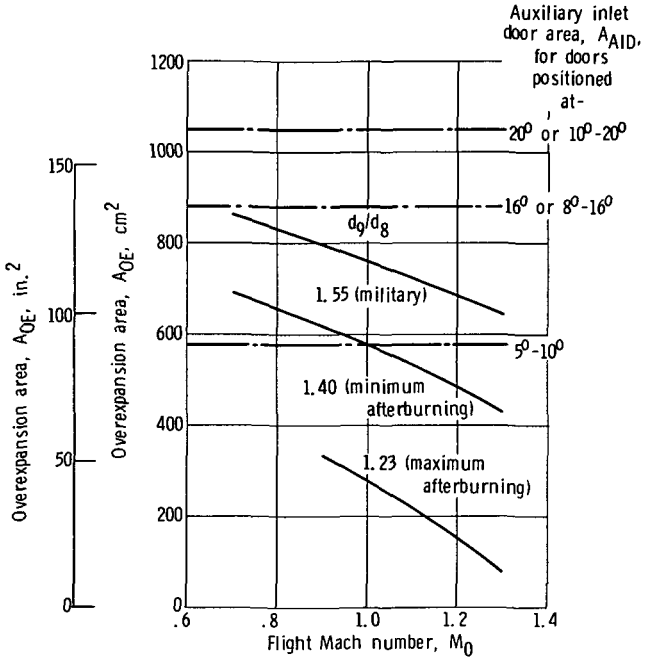

(b) Overexpansion area.

Figure 7. - Geometric characteristics of ejector nozzle.

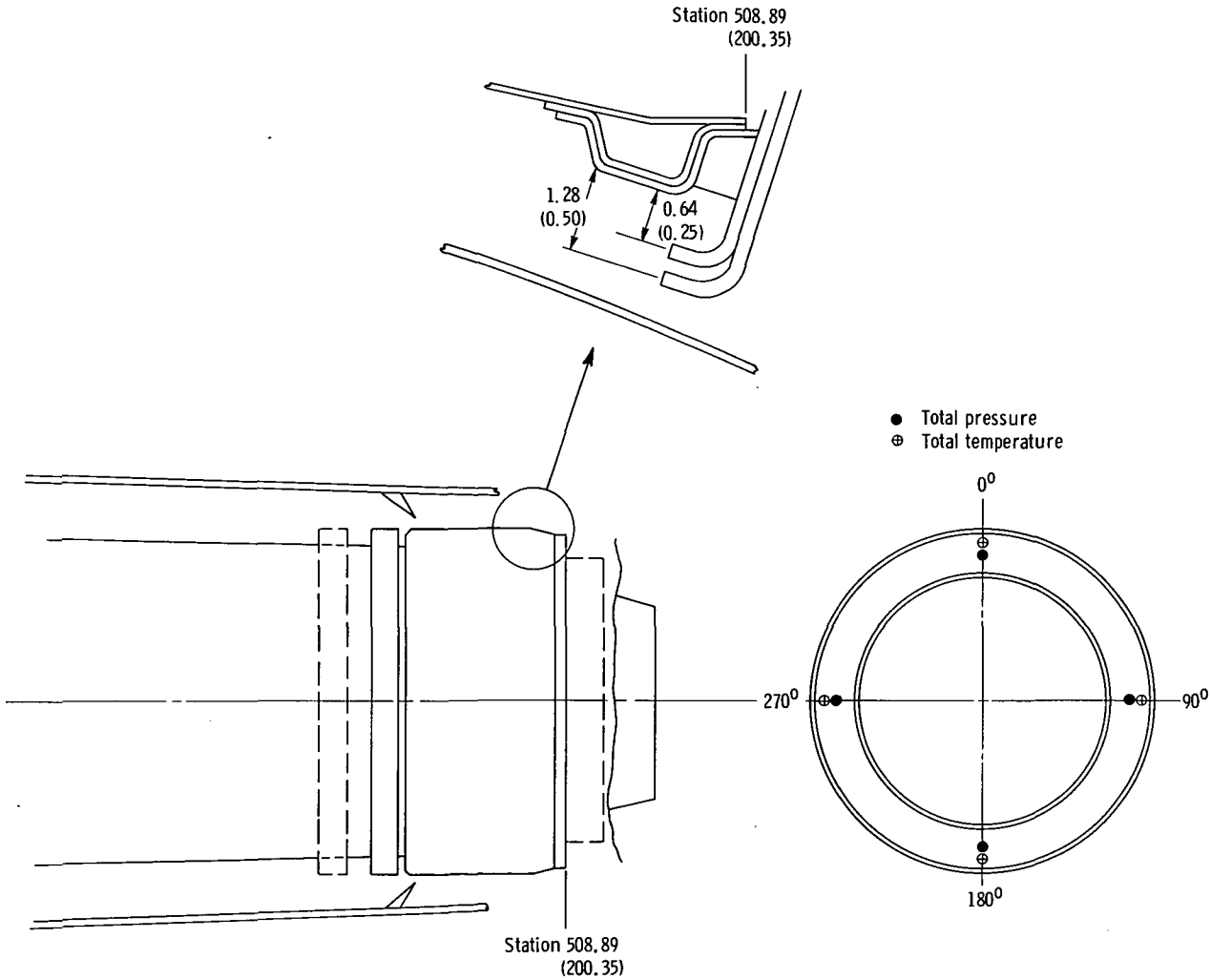

Figure 8. - Secondary passage instrumentation. (Dimensions are in cm (in.).)

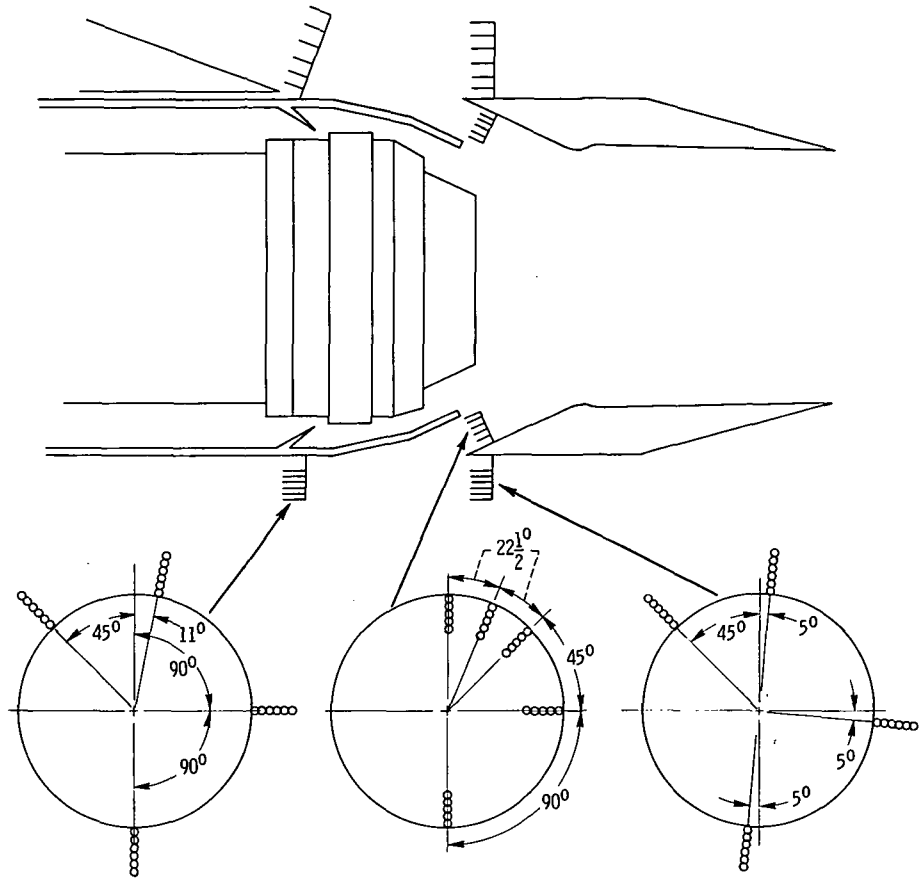

Boundary-layer rakes (station 480.92 (189.34))

Tertiary rakes (station 521.03 (205.13))

Boundary-layer rakes (station 519.35 (204.47))

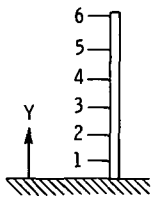

Tube	Y/d_n
1	0.0114
2	.0342
3	.0684
4	.114
5	.171
6	.24

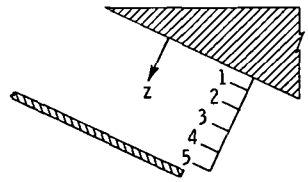

Tube	z/d_n
1	0.011
2	.0329
3	.055
4	.077
5	.0991

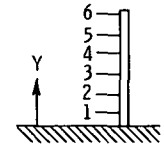

Tube	Y/d_n
1	0.0059
2	.017
3	.0342
4	.0568
5	.0848
6	.12

Boundary-layer rakes near top of nozzle

Tertiary rakes

Boundary-layer rakes at other locations

(a) Boundary-layer and tertiary rakes.

Figure 9. -Ejector nozzle instrumentation details. (Dimensions are in cm (in.).)

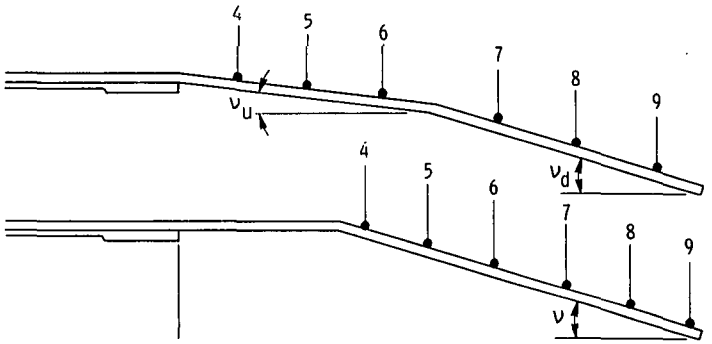

Instrumentation number	Station					
	cm	in.	cm	in.	cm	in.
	Door position, deg					
	$\nu_u = 5^0$, $\nu_d = 10^0$		$\nu_u = 8^0$, $\nu_d = 16^0$		$\nu_u = 10^0$, $\nu_d = 20^0$	
4	491.41	193.47	491.39	193.46	491.39	193.46
5	496.47	195.46	496.44	195.45	496.37	195.42
6	501.52	197.45	501.45	197.42	501.42	197.41
7	506.55	199.43	506.4	199.37	506.27	199.32
8	511.56	201.4	511.30	201.3	511.02	201.19
9	516.56	203.37	516.18	203.22	515.8	203.07
	Door position, deg					
	$\nu = 16^0$		$\nu = 20^0$			
4	498.4	196.22	498.4	196.22		
5	502.08	197.67	502.01	197.64		
6	505.74	199.11	505.61	199.06		
7	509.45	200.57	509.22	200.48		
8	513.11	202.01	512.83	201.9		
9	516.79	203.46	516.41	203.31		

(b) Auxiliary inlet door external static pressures. Circumferential location of instrumented doors, 0^0, $22\frac{1}{2}^0$, 45^0, 90^0, 180^0 (looking upstream).

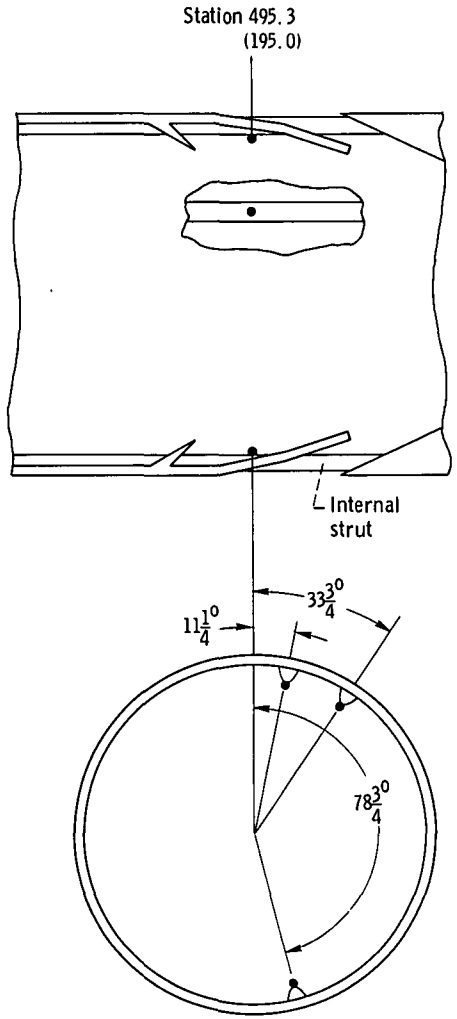

(c) Auxiliary inlet door internal static pressures.

Figure 9. - Continued.

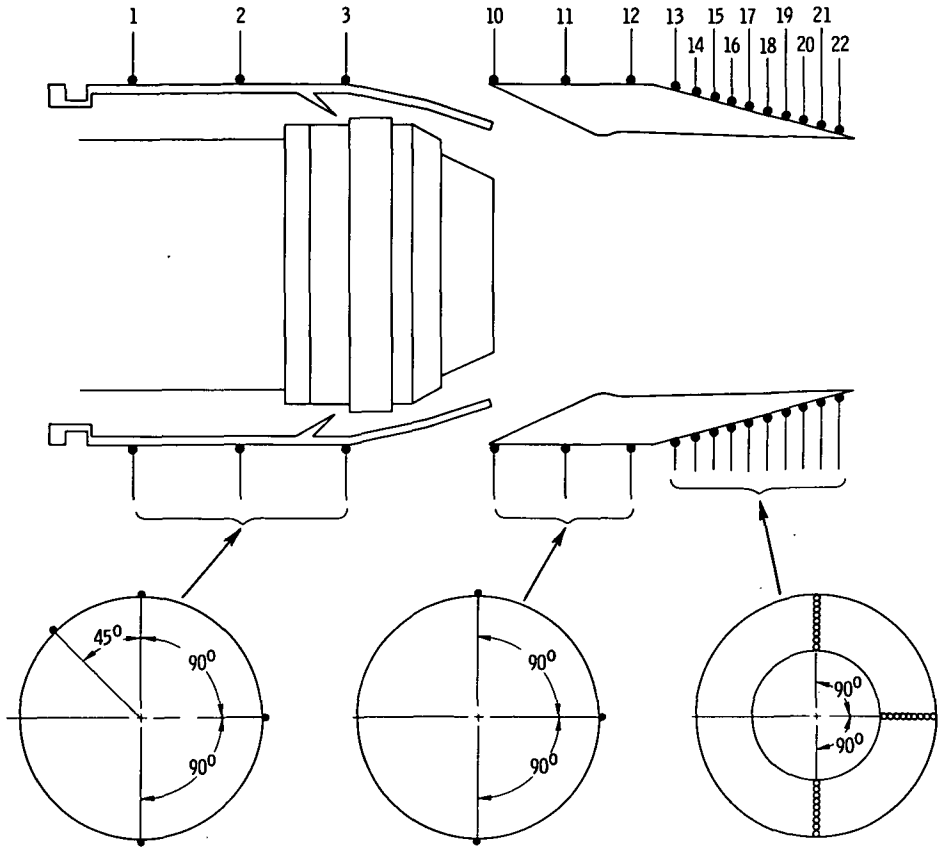

Looking upstream

Instrumentation number	Station	
	cm	in.
1	472.62	186.07
2	480.92	189.34
3	488.87	192.47
10	519.35	204.47
11	539.67	212.47
12	559.99	220.47
13	562.91	221.62
14	566.42	223.00

Instrumentation number	Station	
	cm	in.
15	569.26	224.12
16	572.19	225.27
17	575.18	226.45
18	578.28	227.67
19	581.46	228.92
20	584.76	230.22
21	588.16	231.56
22	591.29	232.79

(d) External static pressures.

Figure 9. - Continued.

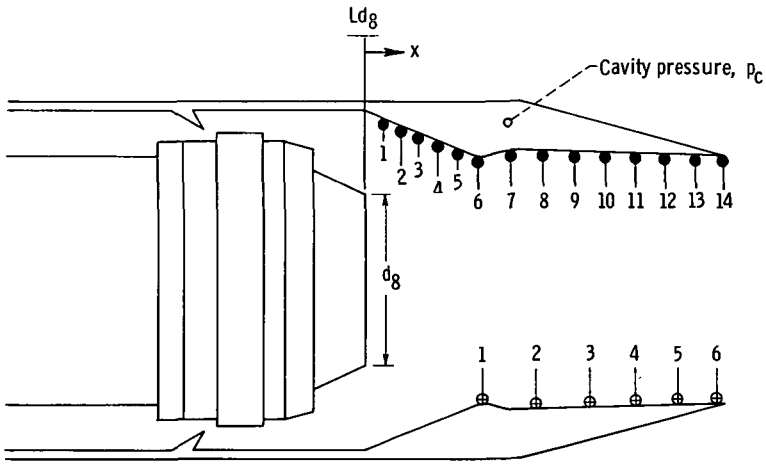

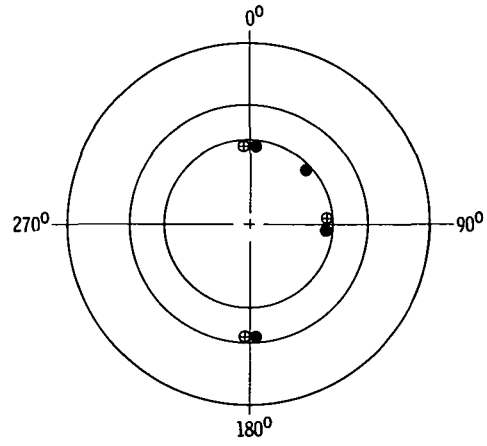

Looking upstream

Instrumentation number	Station	
	cm	in.
Pressure		
1	521.03	205.13
2	523.67	206.17
3	527.99	207.87
4	532.31	209.57
5	536.63	211.27
6	540.94	212.97
7	547.5	215.55
8	554.0	218.11
9	560.5	220.67
10	567.00	223.23
11	573.51	225.79
12	580.01	228.35
13	586.51	230.91
14	593.01	233.47

Instrumentation number	Station	
	cm	in.
Temperature		
1	540.94	212.97
2	551.36	217.07
3	561.77	221.07
4	572.19	225.27
5	582.6	229.37
6	593.01	233.47

● Pressure
⊕ Temperature

(e) Internal static pressures and wall temperatures. (x = Station - Ld_8, $Ld_8 = f(A_8)$, see fig. 3.)

Figure 9. - Concluded.

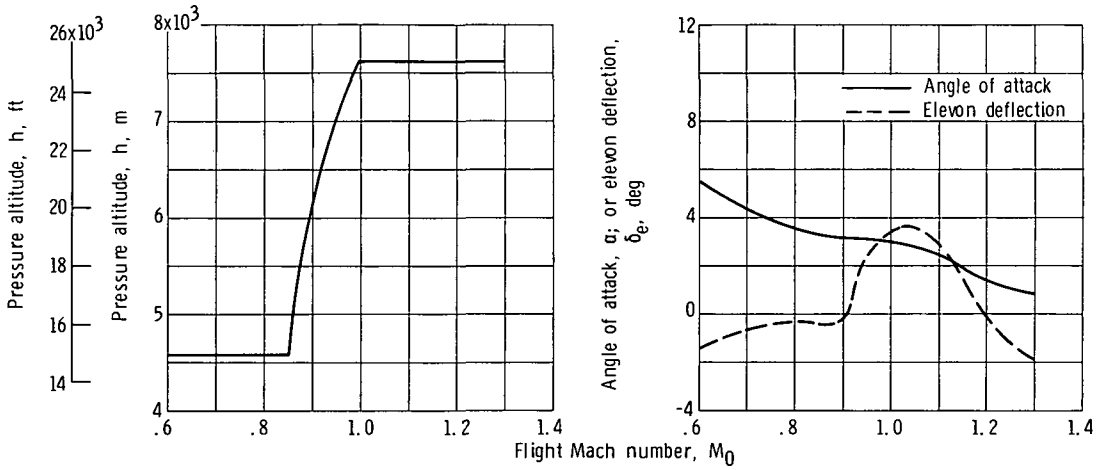

(a) Nominal flight test altitude - Mach number profile.

(b) Nominal angle of attack and elevon deflection with Mach number.

Figure 10. - Flight conditions.

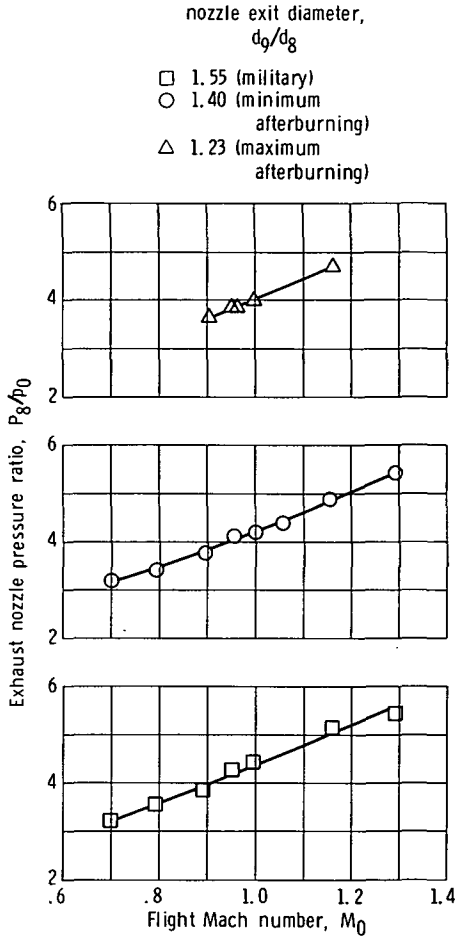

(c) Exhaust nozzle pressure ratio schedule.

Figure 10. - Concluded.

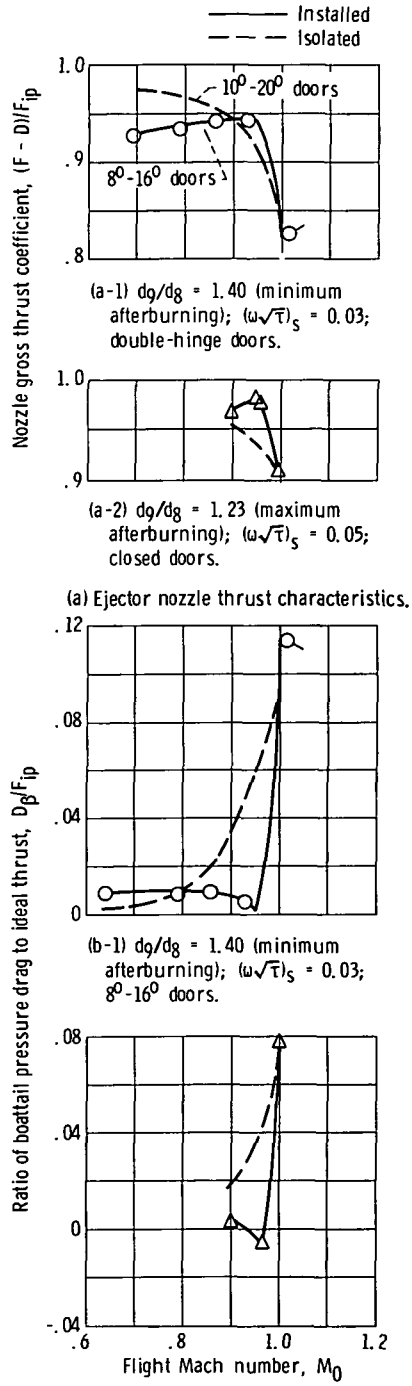

(a-1) d_9/d_8 = 1.40 (minimum afterburning); $(\omega\sqrt{\tau})_s$ = 0.03; double-hinge doors.

(a-2) d_9/d_8 = 1.23 (maximum afterburning); $(\omega\sqrt{\tau})_s$ = 0.05; closed doors.

(a) Ejector nozzle thrust characteristics.

(b-1) d_9/d_8 = 1.40 (minimum afterburning); $(\omega\sqrt{\tau})_s$ = 0.03; 8°-16° doors.

(b-2) d_9/d_8 = 1.23 (maximum afterburning); $(\omega\sqrt{\tau})_s$ = 0.05; closed doors.

(b) Boattail drag.

Figure 11. - Installation effect on peak performance as function of Mach number.

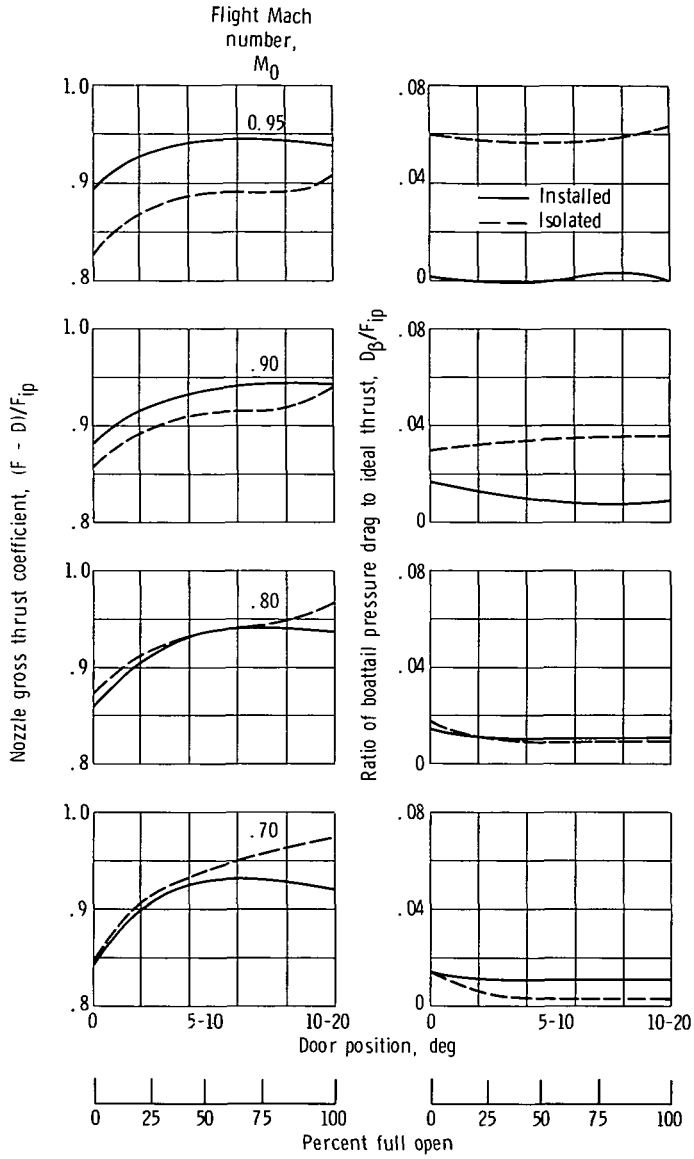

Figure 12. - Installation effect as function of door position. Double-hinge doors; $d_9/d_8 = 1.40$ (minimum afterburning); $(\omega\sqrt{\theta})_s = 0.035$.

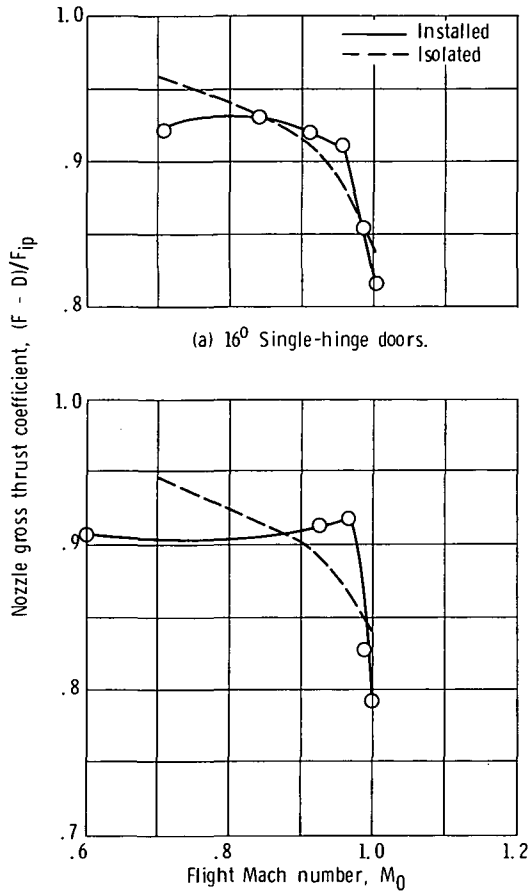

Figure 13. - Installation effect on nozzle gross thrust as function of Mach number. Single-hinge doors; $d_9/d_8 = 1.40$ (minimum afterburner; $(\omega\sqrt{\tau})_s = 0.035$.

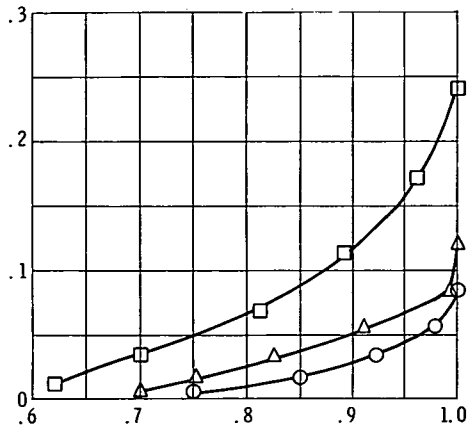

(a) $M_0 = 0.69$; $(\omega\sqrt{\tau})_s = 0.029$.

Ratio of boundary-layer momentum thickness to nozzle maximum diameter, δ^{**}/d_n	Ratio of local-free-stream to free-stream velocity, V_L/V_0	Rake location, deg
□ 0.0224	1.0727	11
○ .0052	1.0289	90
△ .0092	1.0266	180
.0134 (isolated)		

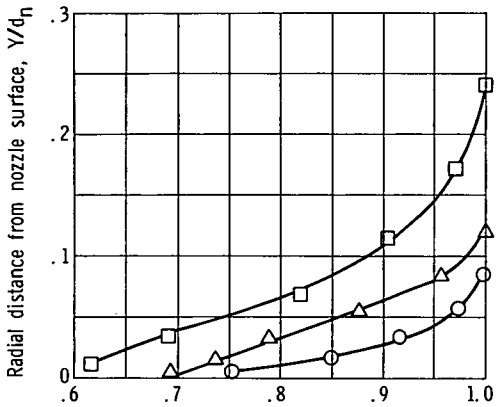

(b) $M_0 = 0.79$; $(\omega\sqrt{\tau})_s = 0.031$.

Ratio of boundary-layer momentum thickness to nozzle maximum diameter, δ^{**}/d_n	Ratio of local-free-stream to free-stream velocity, V_L/V_0	Rake location, deg
□ 0.0209	1.0893	11
○ .0054	1.0205	90
△ .0114	.9667	180
.0134 (isolated)		

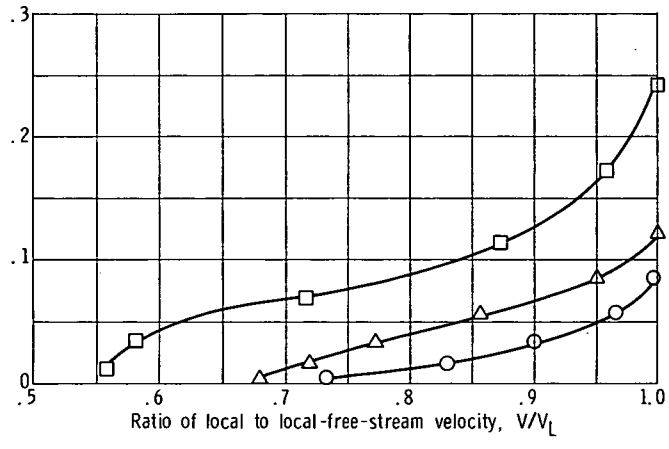

(c) $M_0 = 0.86$; $(\omega\sqrt{\tau})_s = 0.031$.

Ratio of boundary-layer momentum thickness to nozzle maximum diameter, δ^{**}/d_n	Ratio of local-free-stream to free-stream velocity, V_L/V_0	Rake location, deg
□ 0.0255	1.0960	11
○ .0061	1.0243	90
△ .0121	1.0049	180
.015 (isolated)		

Figure 14. - Boundary-layer velocity profile upstream of auxiliary inlet doors. 8^0 - 16^0 double-hinge doors.

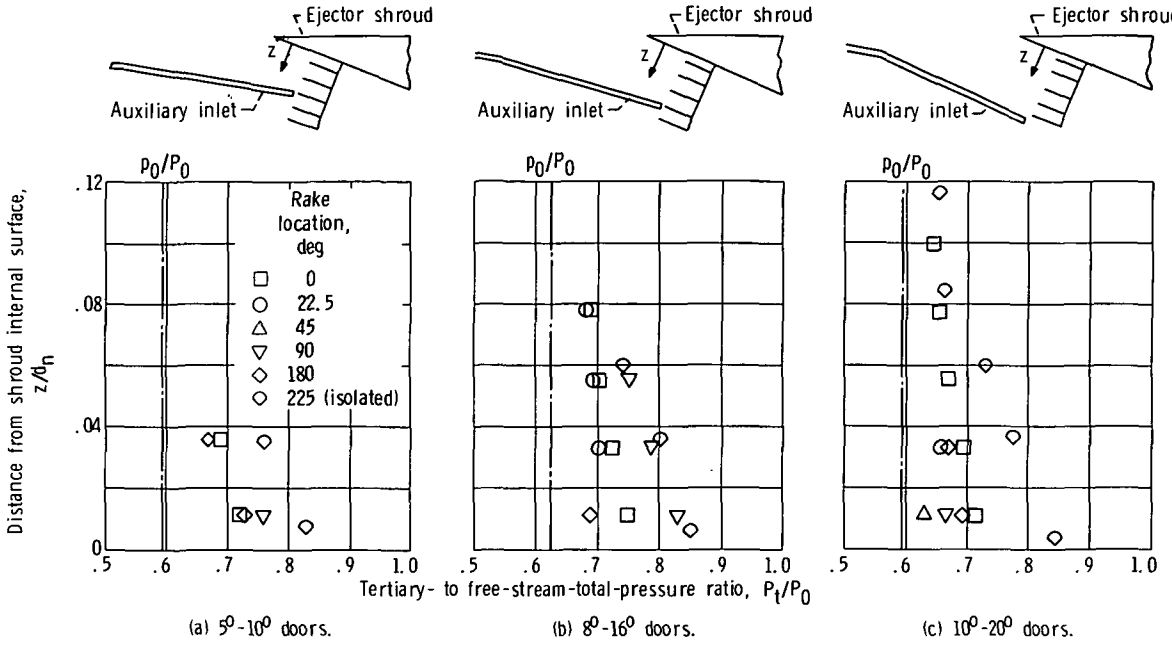

Figure 15. - Total-pressure recovery inside entrance to auxiliary inlet doors. Conditions: d_9/d_8 = 1.40 (minimum afterburning); M_0 = 0.9; $(\omega\sqrt{\tau})_s$ = 0.035.

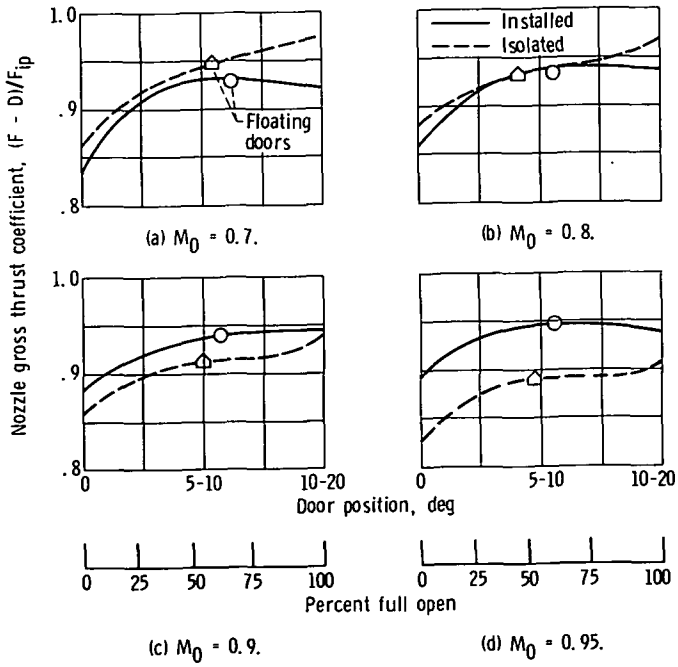

Figure 16. - Installation effect on performance of floating door configuration. Conditions: d_9/d_8 = 1.40 (minimum afterburning); $(\omega\sqrt{\tau})_s$ = 0.03.

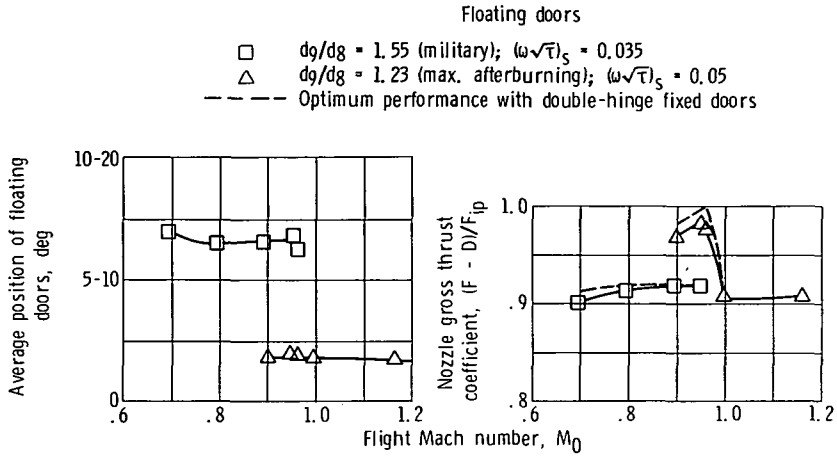

Figure 17. - Comparison of optimum and floating-door performance of installed nozzle.

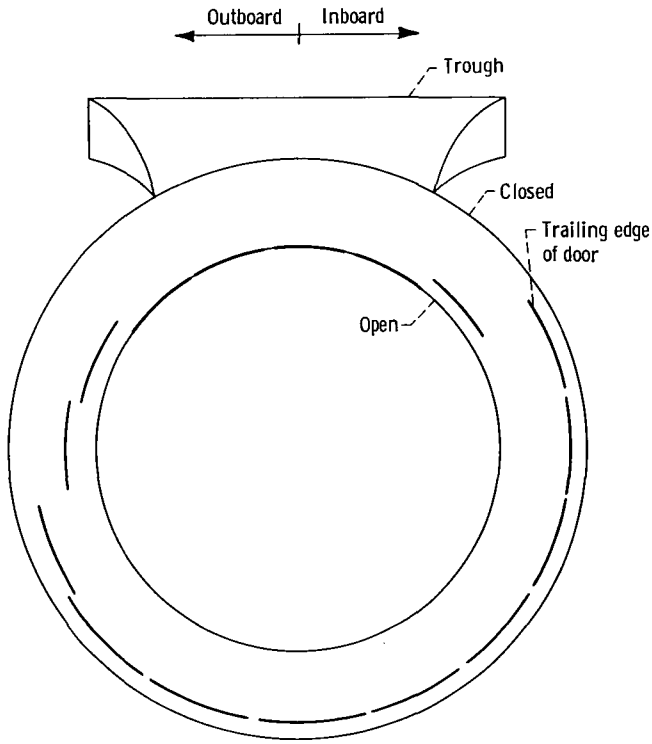

Figure 18. - Positions of floating doors. Conditions: d_9/d_8 = 1.40 (minimum afterburning); M_0 = 0.9; $(\omega\sqrt{\tau})_S$ = 0.035.

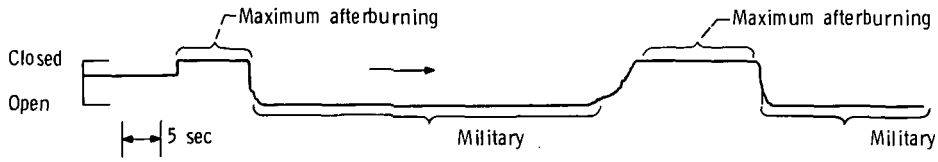

Figure 19. - Response of floating door to changes in power setting. Conditions: $M_0 = 0.9$; $(\omega\sqrt{\tau})_s = 0.05$; bottom door.

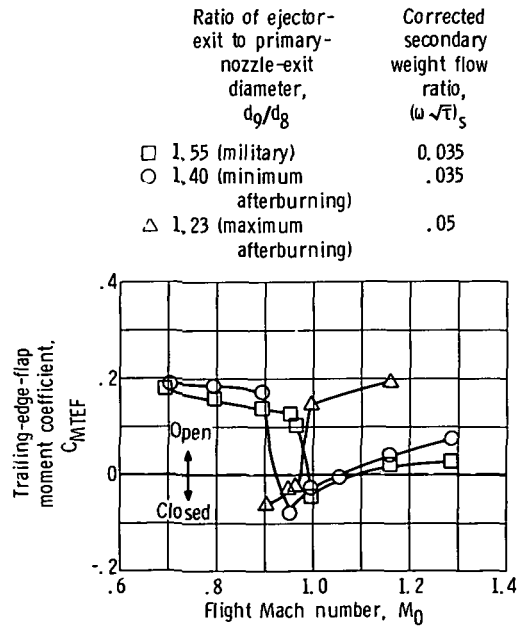

Figure 20. - Effect of Mach number on trailing-edge-flap moment coefficient for floating doors.

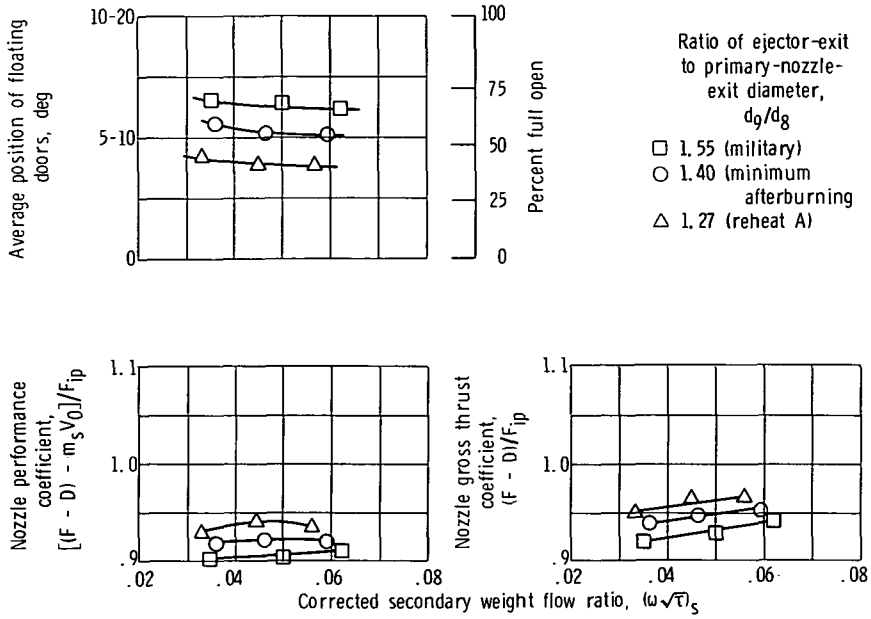

Figure 21. - Thrust characteristics and floating door position as function of corrected secondary weight flow ratio. Floating doors; $M_0 = 0.9$.

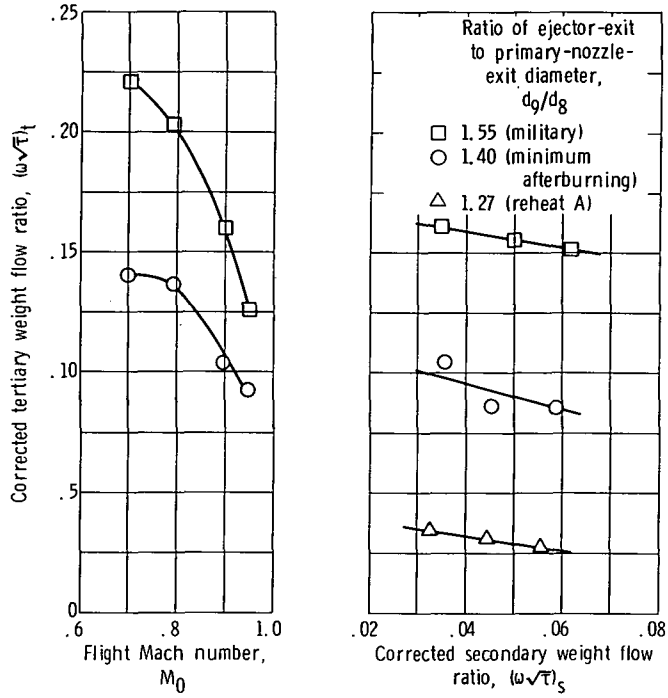

(a) As function of M_0; $(\omega\sqrt{\tau})_s = 0.035$.

(b) As function of $(\omega\sqrt{\tau})_s$; $M_0 = 0.9$.

Figure 22. - Estimated corrected tertiary weight flow ratio for floating doors.

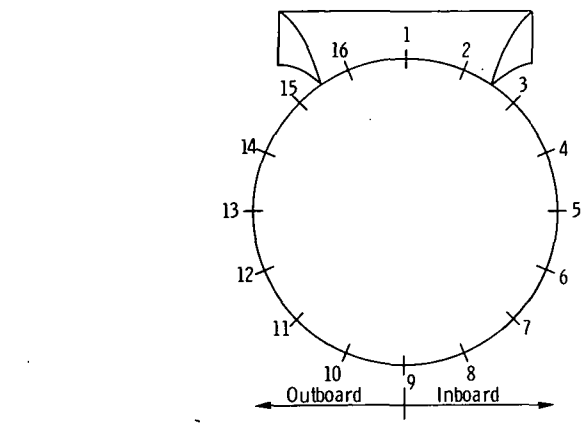

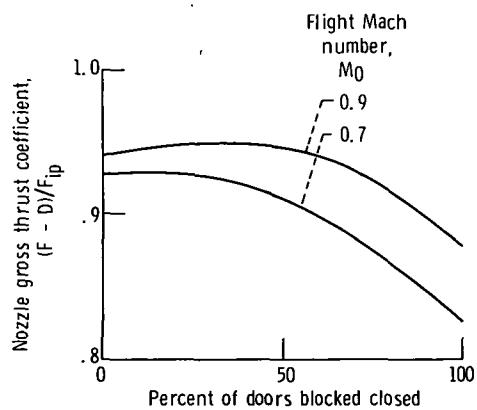

Percent closed	Doors closed
18.75	1, 2, 16
18.75	3, 9, 15
43.75	3, 4, 8, 9, 10, 14, 15
100	All

Figure 23. - Effect of door blockage on nozzle gross thrust coefficient. Conditions: $d_9/d_8 = 1.40$ (minimum afterburning); $(\omega\sqrt{T})_S = 0.035$.

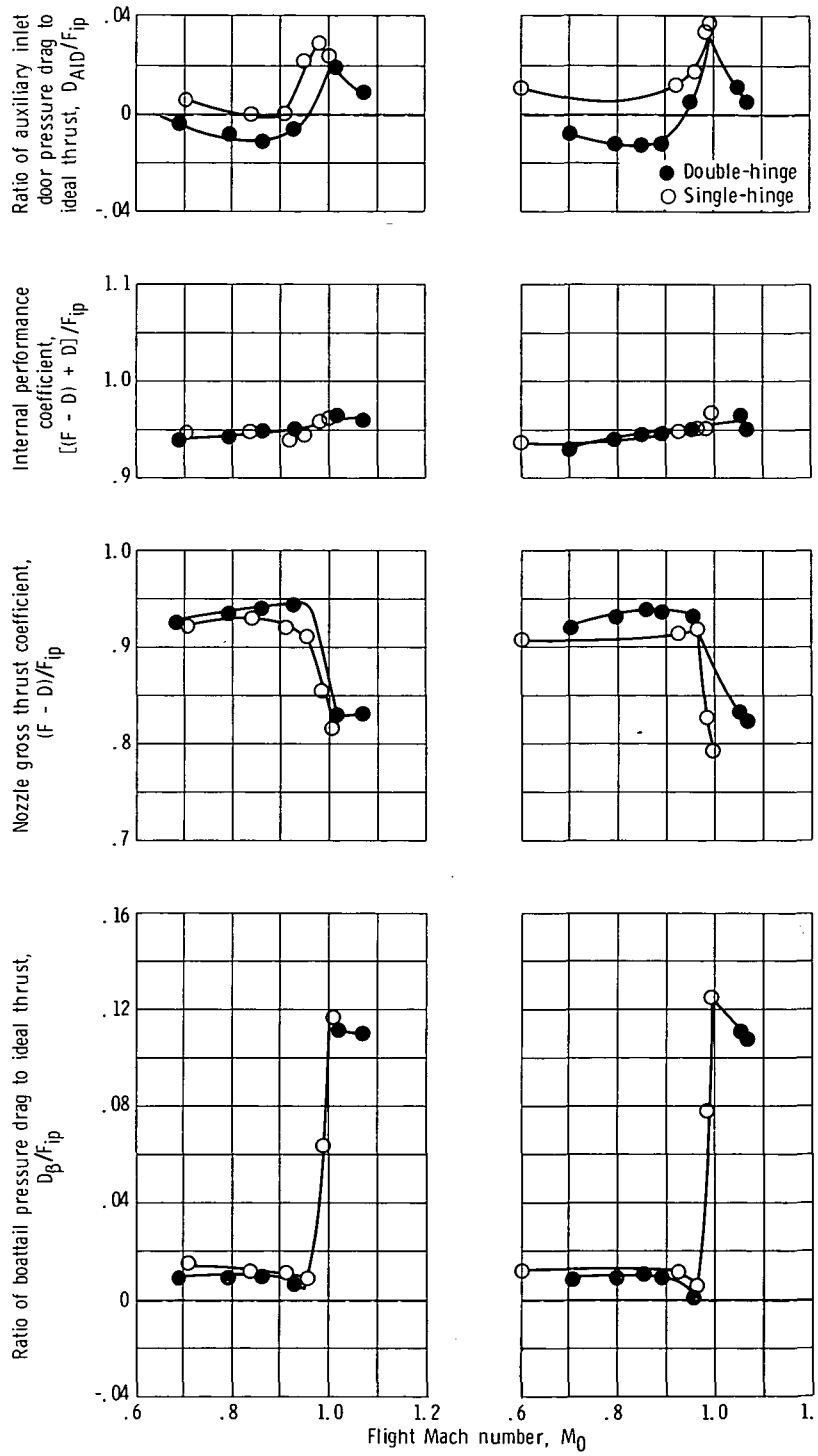

(a) 16^0 and 16^0-18^0 open doors. (b) 20^0 and 10^0-20^0 open doors.

Figure 24. - Comparison of ejector nozzle performance and pressure drag to ideal gross thrust ratios for single- and double-hinge doors. Conditions: $d_9/d_8 = 1.40$ (minimum afterburning); $(\omega\sqrt{\tau})_s = 0.035$.

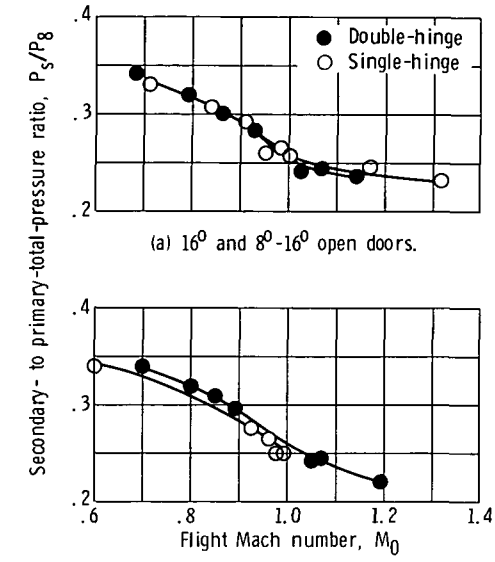

(a) 16^0 and 8^0-16^0 open doors.

(b) 20^0 and 10^0-20^0 open doors.

Figure 25. - Comparison of ejector nozzle pumping performance for single- and double-hinge doors. Conditions: d_9/d_8 = 1.40 (minimum afterburning) $(\omega\sqrt{\bar{T}})_s$ = 0.035.

Ratio of ejector-exit to primary-nozzle-exit diameter, d_9/d_8	Corrected secondary weight flow ratio, $(\omega\sqrt{\bar{T}})_s$
—— 1.23 (maximum afterburning)	0.052
– – 1.40 (minimum afterburning)	.032

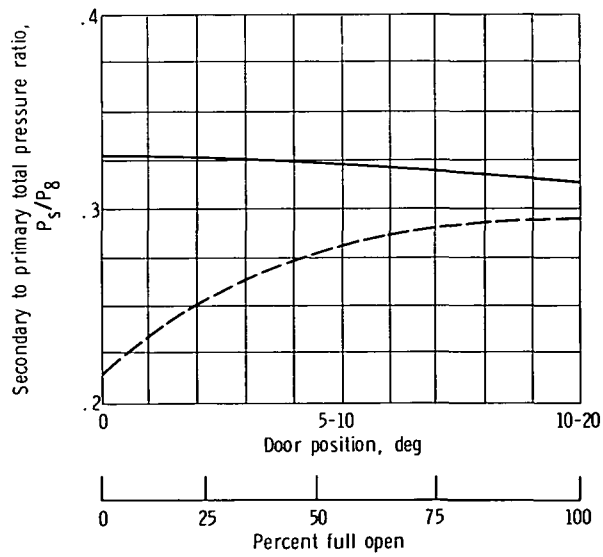

Figure 26. - Pumping performance as function of double-hinge fixed door position. M_0 = 0.9.

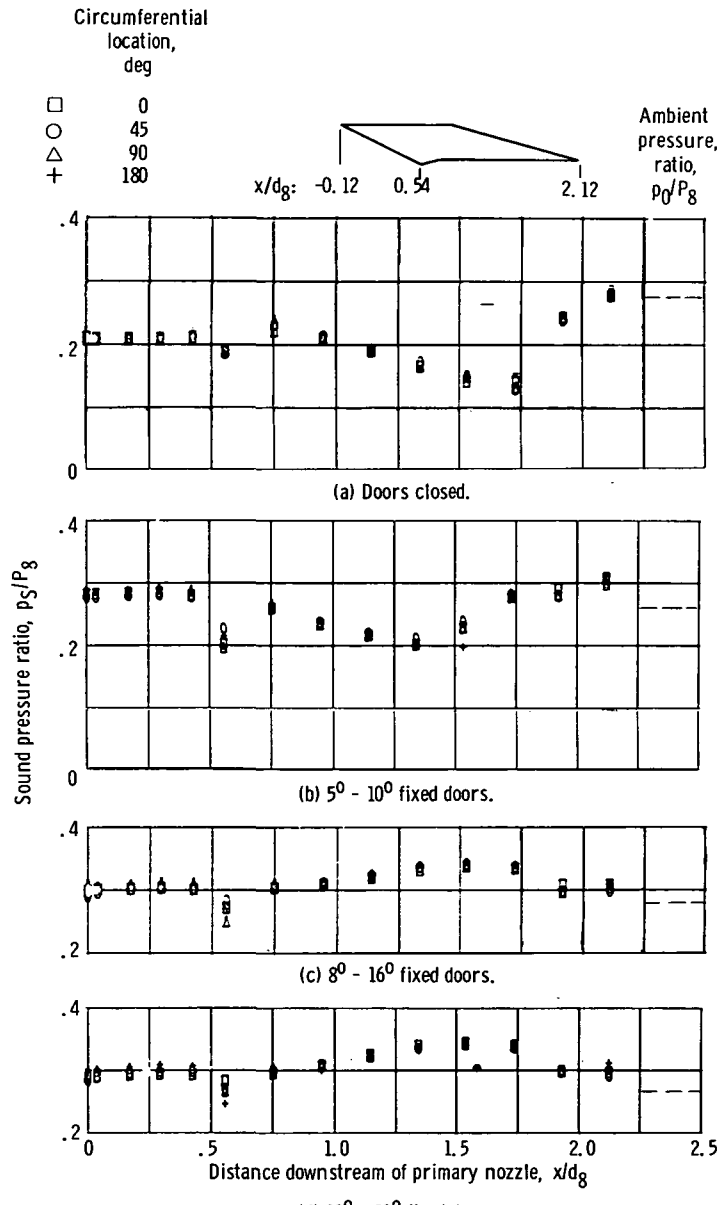

Figure 27. - Static-pressure distribution along interval surface of nozzle. conditions: $d_9/d_8 = 1.40$ (minimum afterburning); $M_0 = 0.9$; $(\omega\sqrt{\tau})_s = 0.032$.

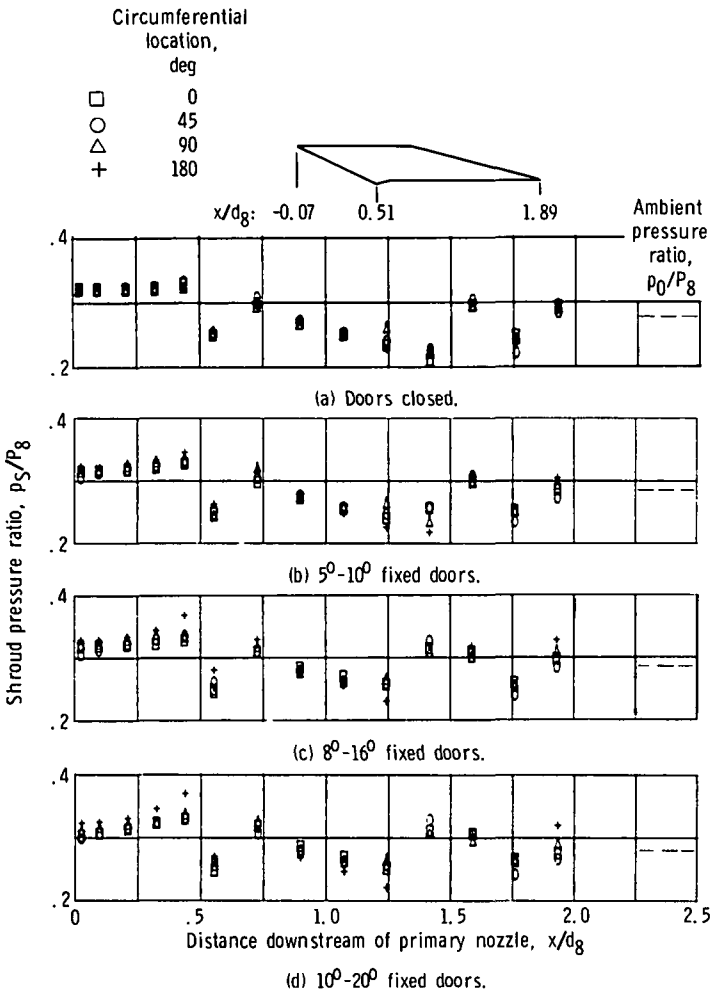

Figure 28. - Static-pressure distribution along internal surface of nozzle. Conditions: d_9/d_8 = 1.23 (maximum afterburning); M_0 = 0.9; $(\omega\sqrt{T})_s$ = 0.052.

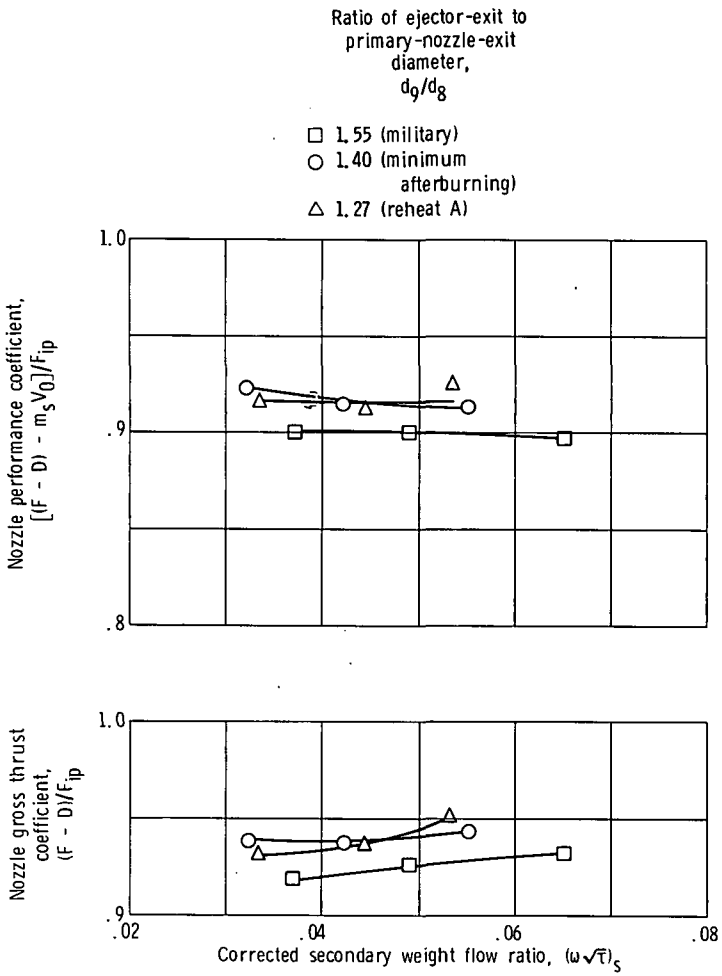

Figure 29. - Ejector nozzle thrust characteristics as function of corrected secondary weight flow ratio. Conditions: 10°-20° open doors; M_0 = 0.9.

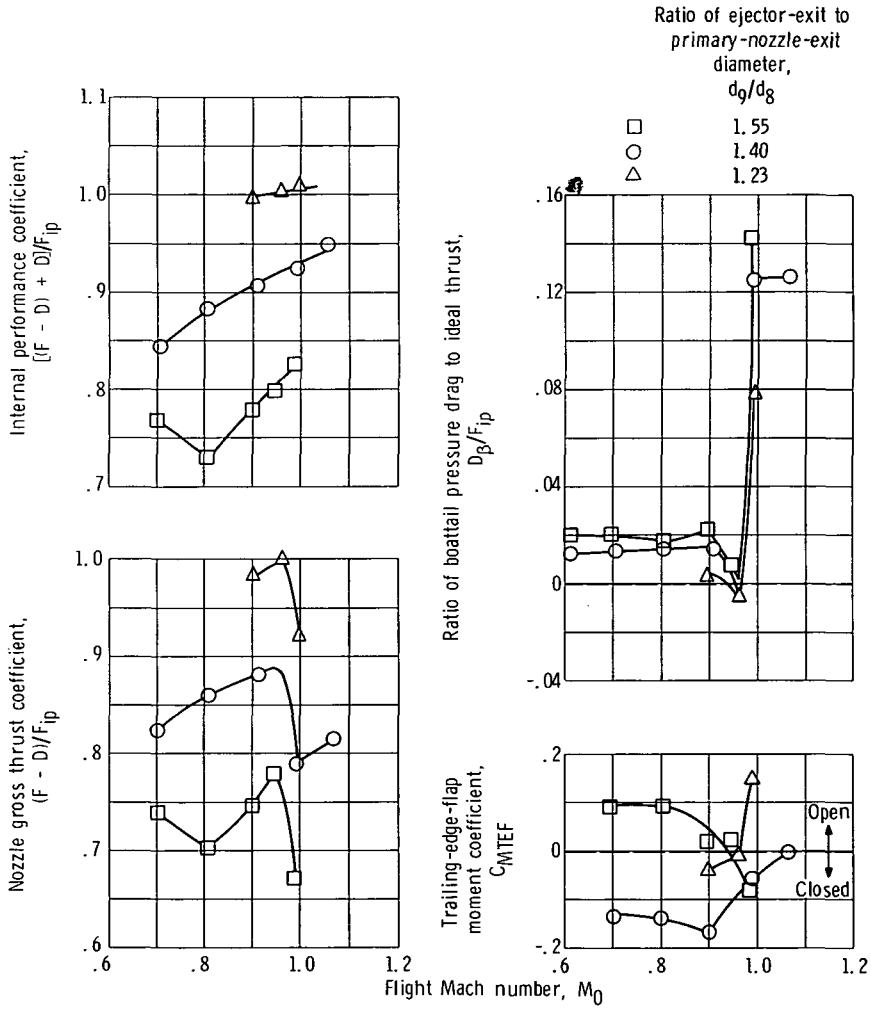

Figure 30. - Ejector nozzle performance characteristics as function of Mach number for closed doors.

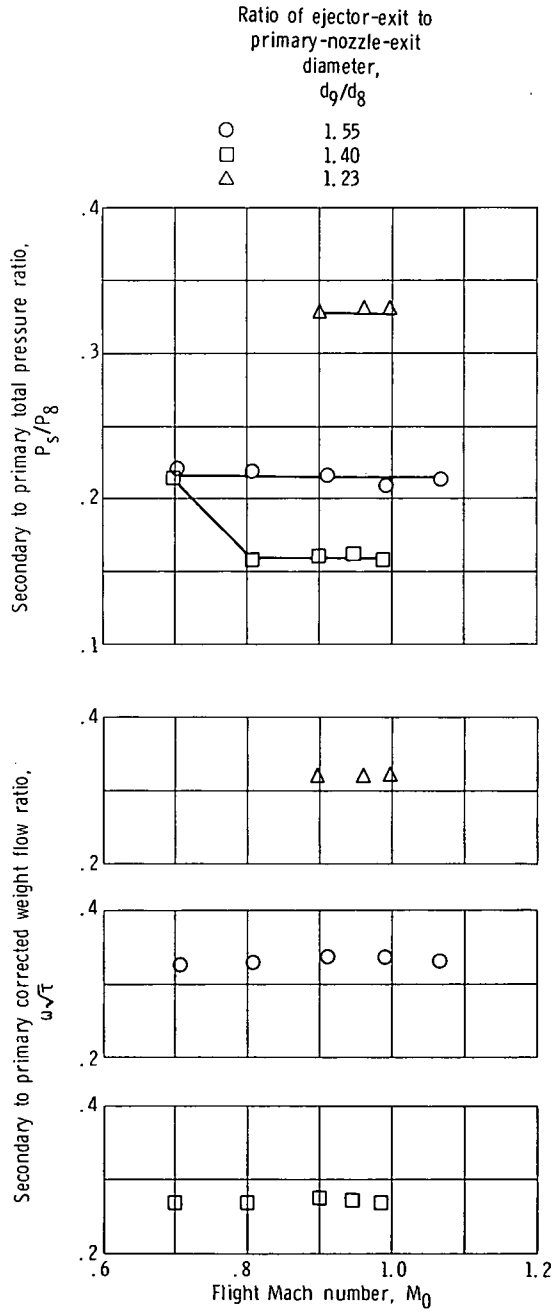

Figure 31. - Ejector nozzle pumping characteristics as function of Mach number for closed doors.

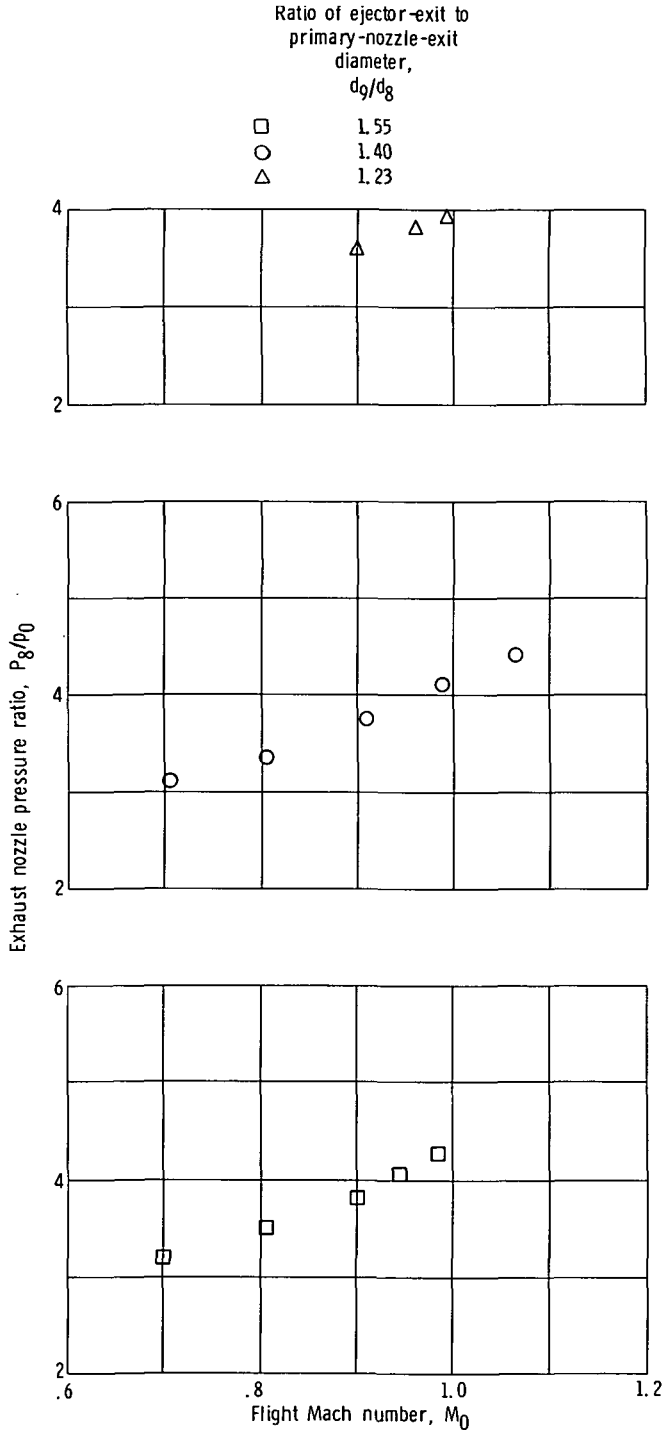

Figure 32. - Nozzle pressure ratio as function of Mach number for closed doors.

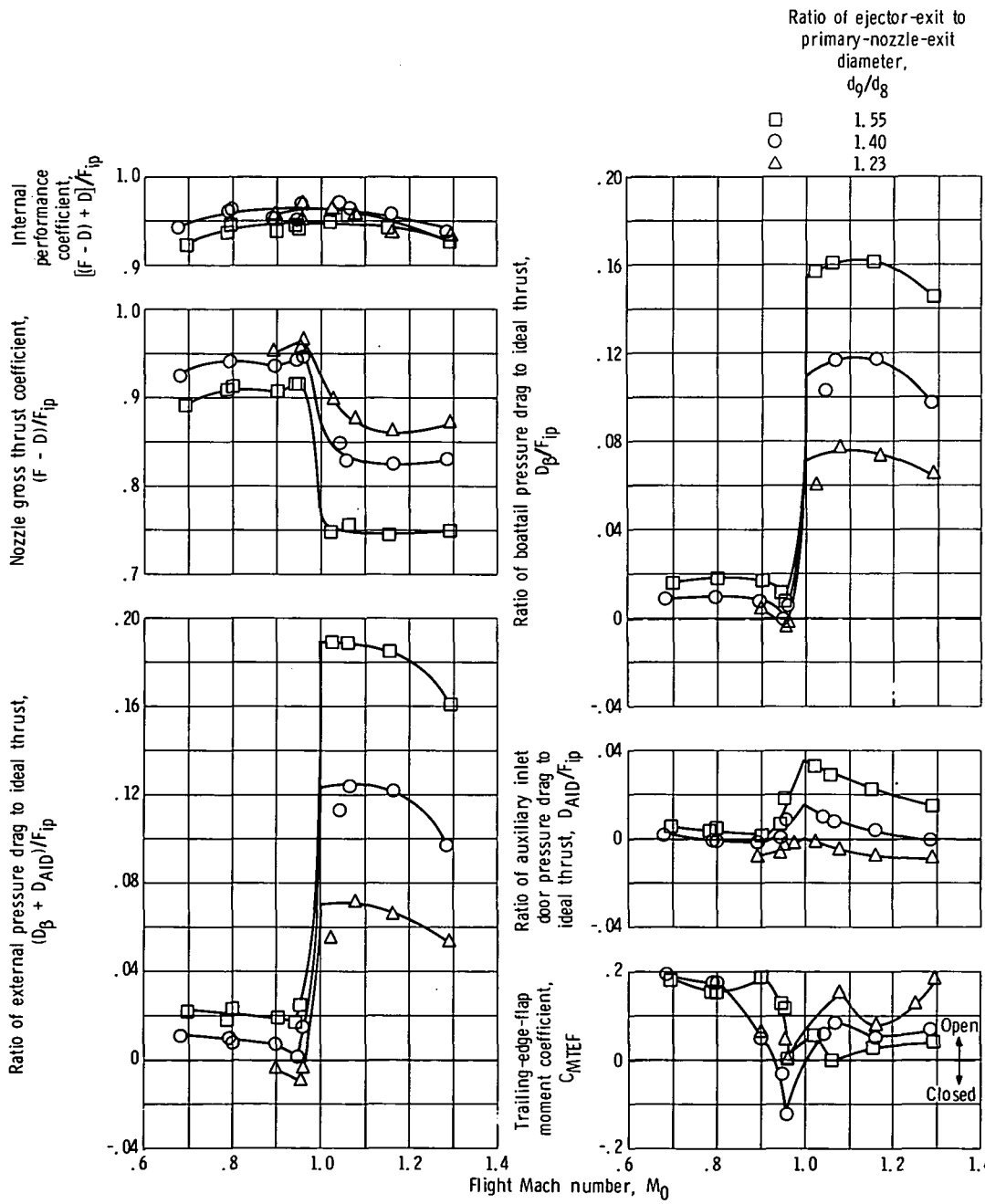

Figure 33. - Ejector nozzle performance characteristics as function of Mach number for 5^0-10^0 doors.

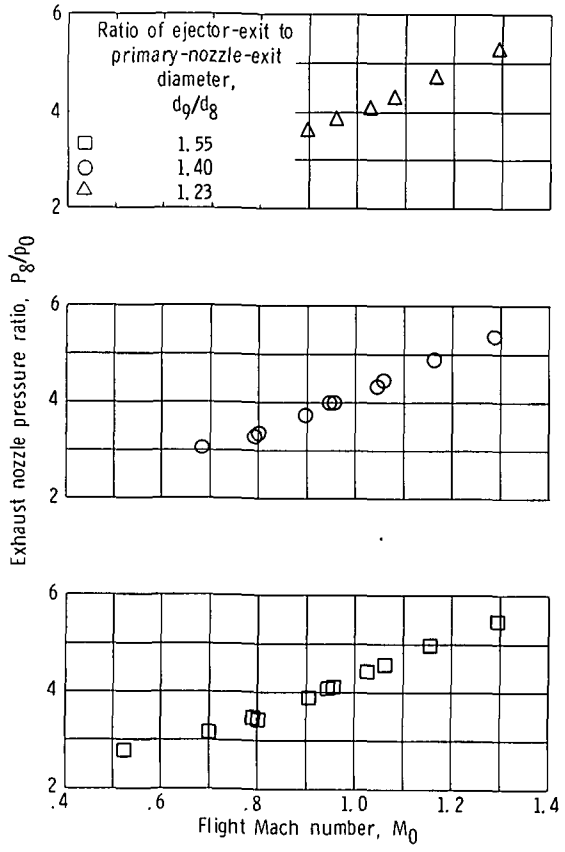

Figure 35. - Nozzle pressure ratio as function of Mach number for 5^0-10^0 doors.

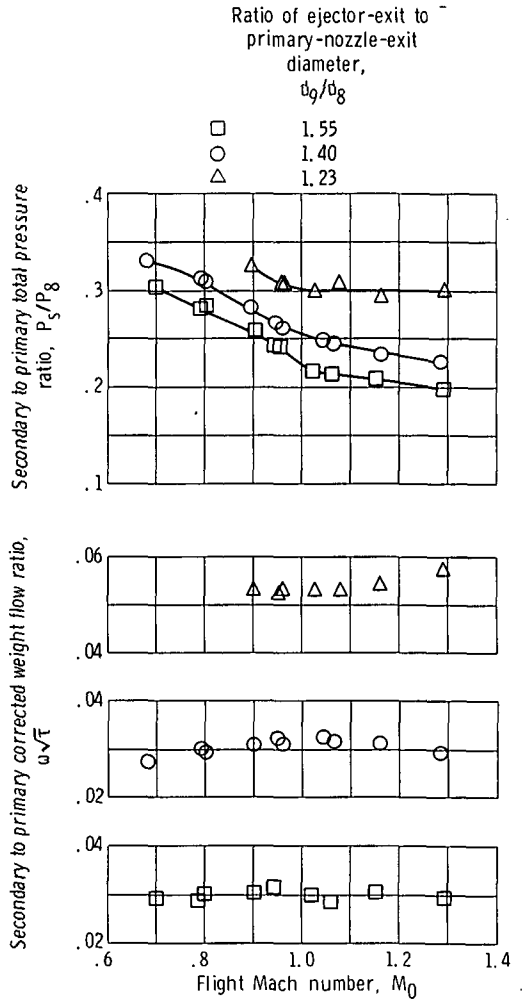

Figure 34. - Ejector nozzle pumping characteristics as function of Mach number for 5^0-10^0 doors.

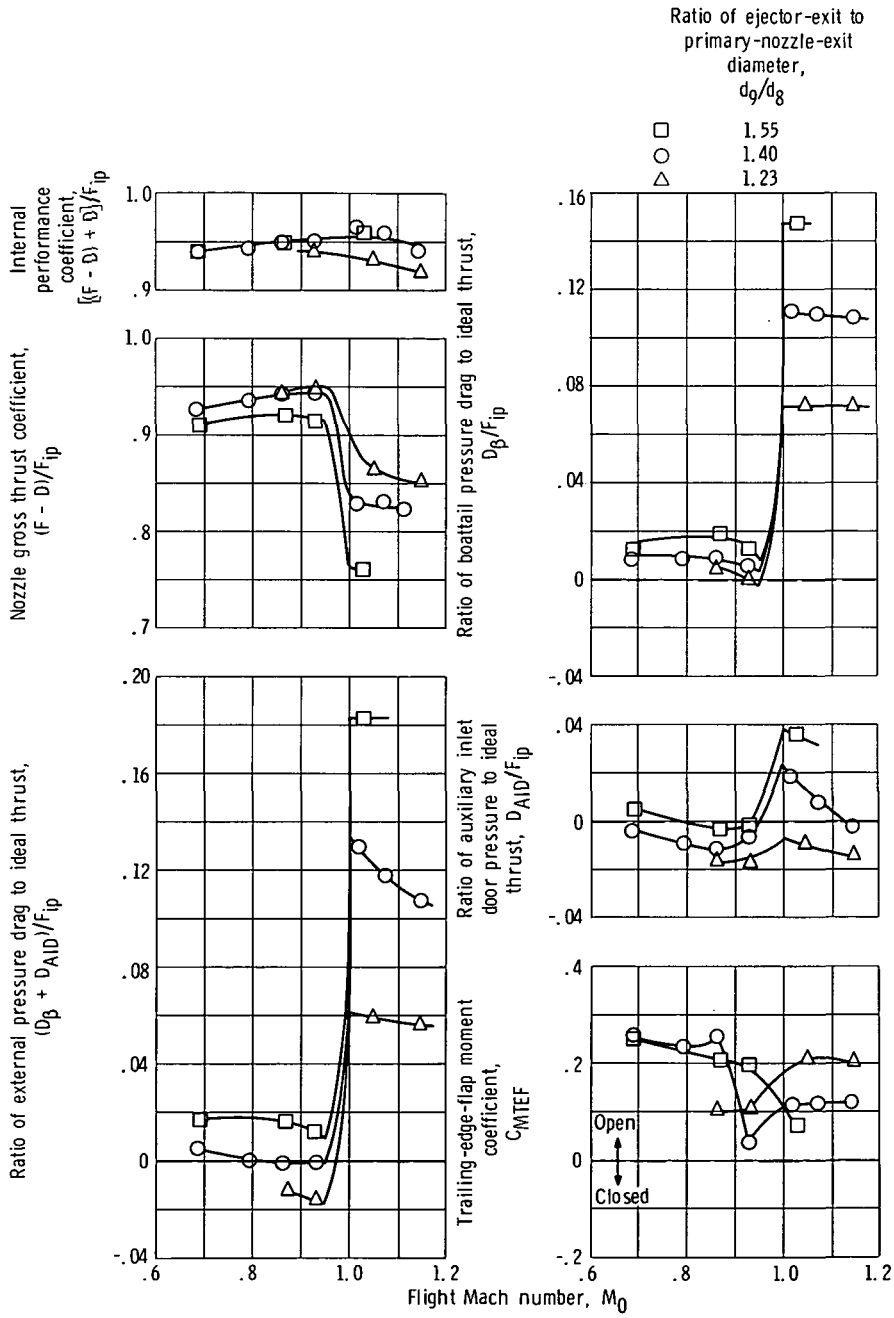

Figure 36. - Ejector nozzle performance characteristics as function of Mach number for 8^0-16^0 doors.

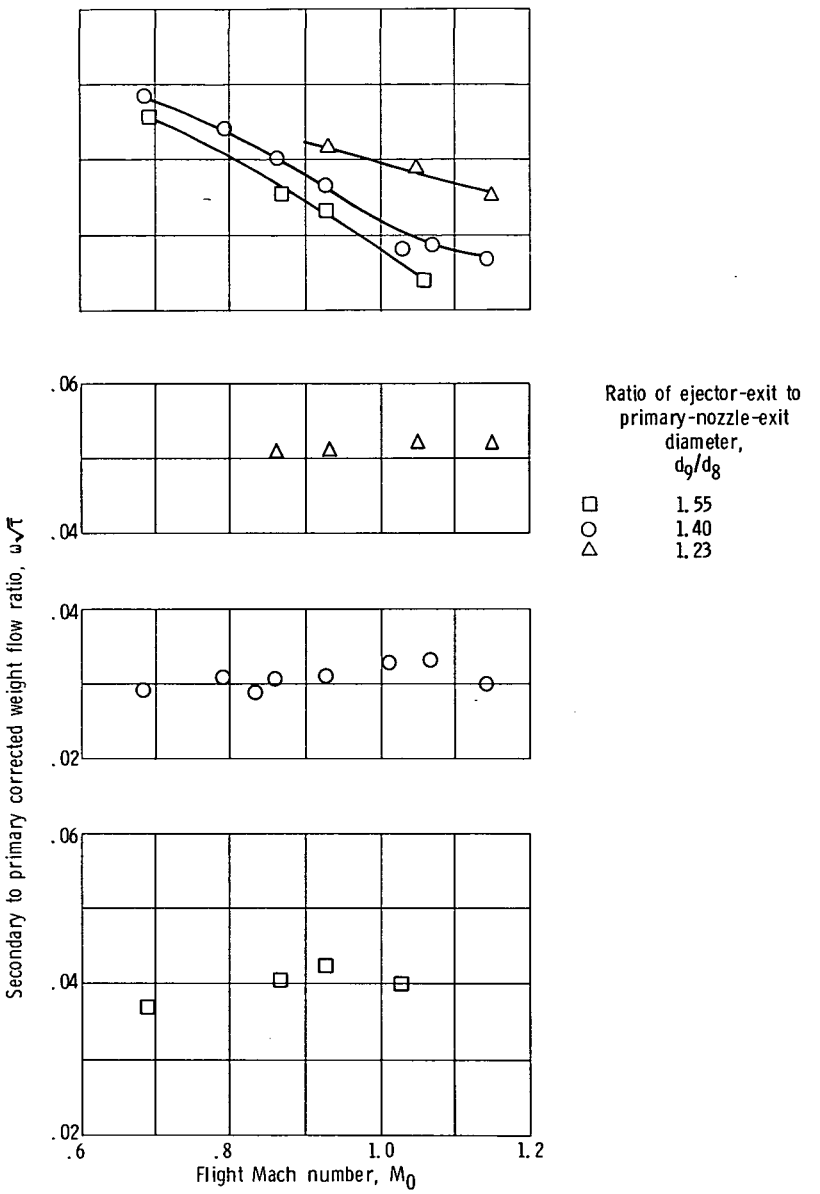

Figure 37. - Ejector nozzle performance characteristics as function of Mach number for 8^0-16^0 doors.

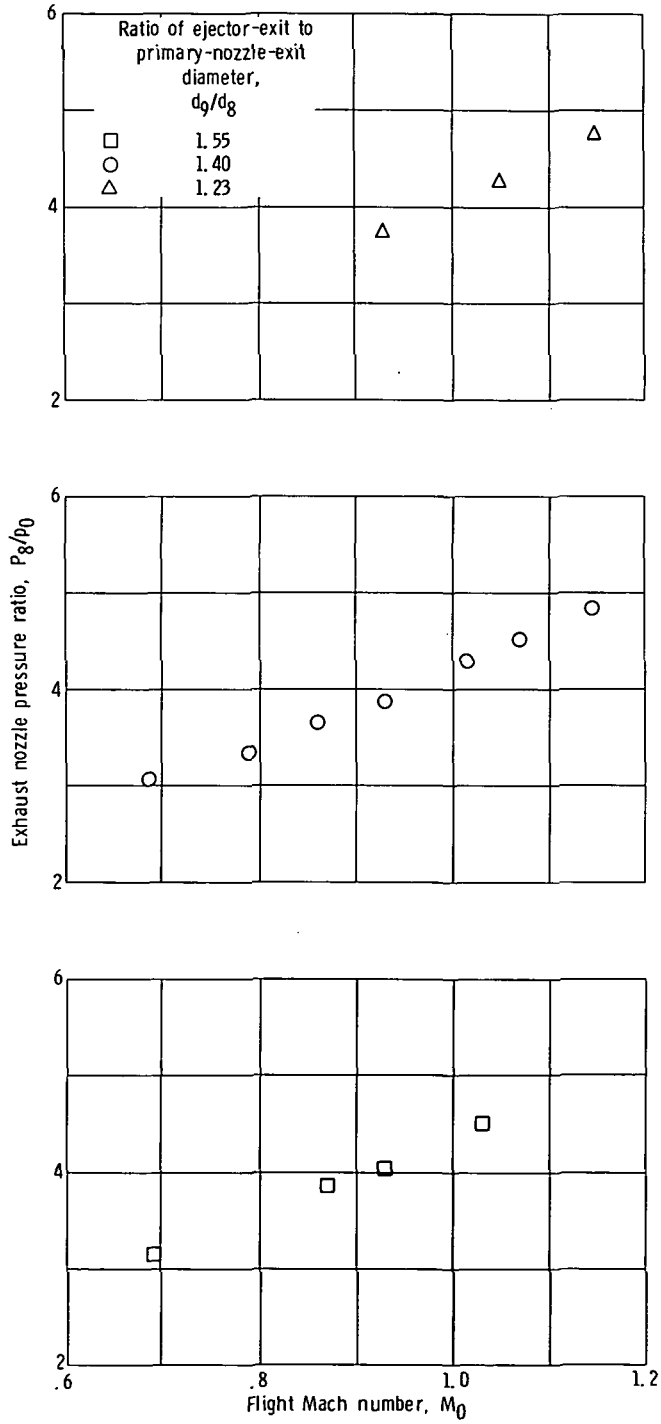

Figure 38. - Nozzle pressure ratio as function of Mach number for 8^0-16^0 doors.

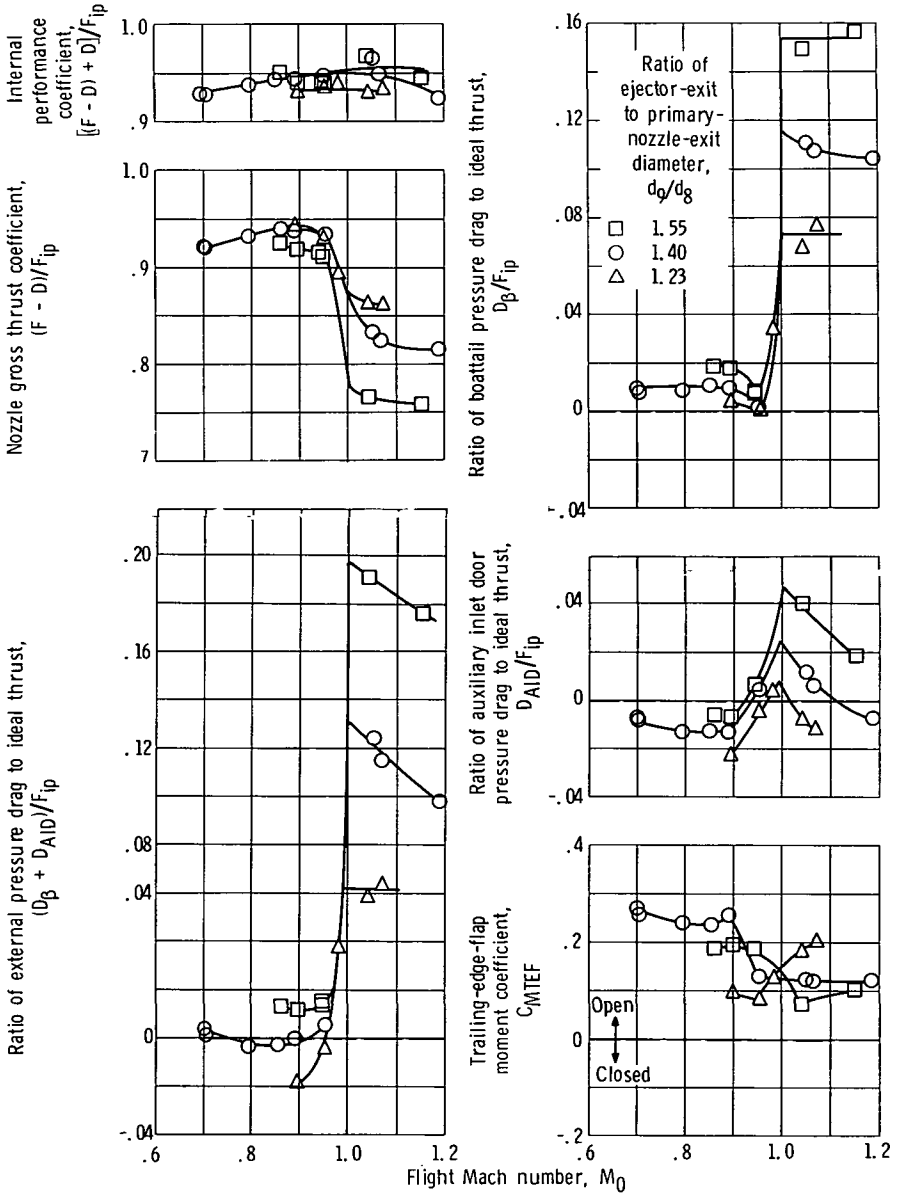

Figure 39. - Ejector nozzle performance characteristics as function of Mach number for 10^0-20^0 doors.

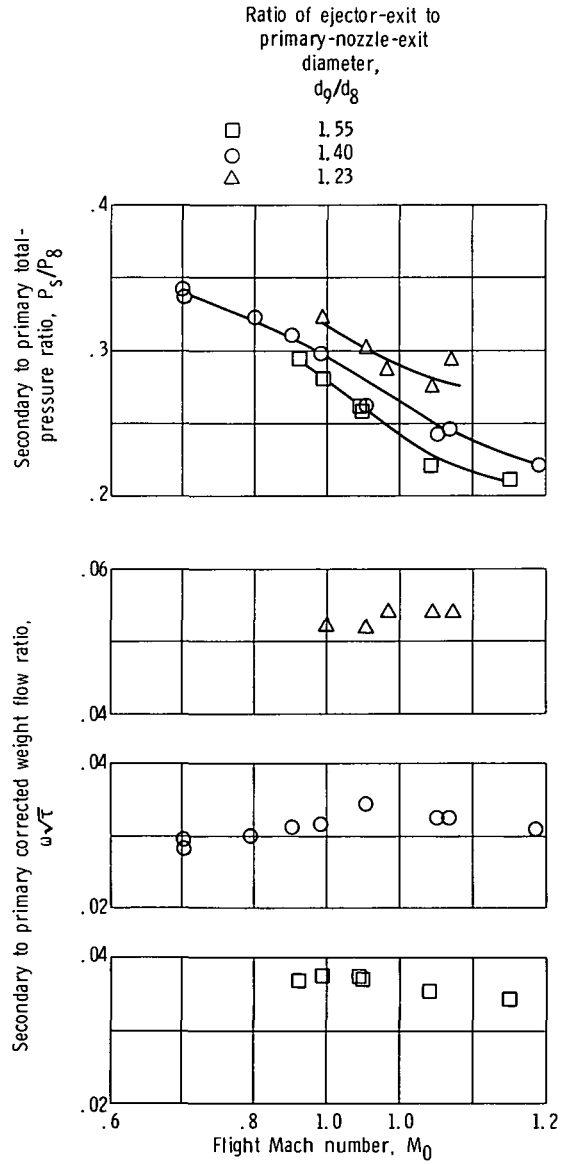

Figure 40. - Ejector nozzle pumping characteristics as function of Mach number for 10^0-20^0 doors.

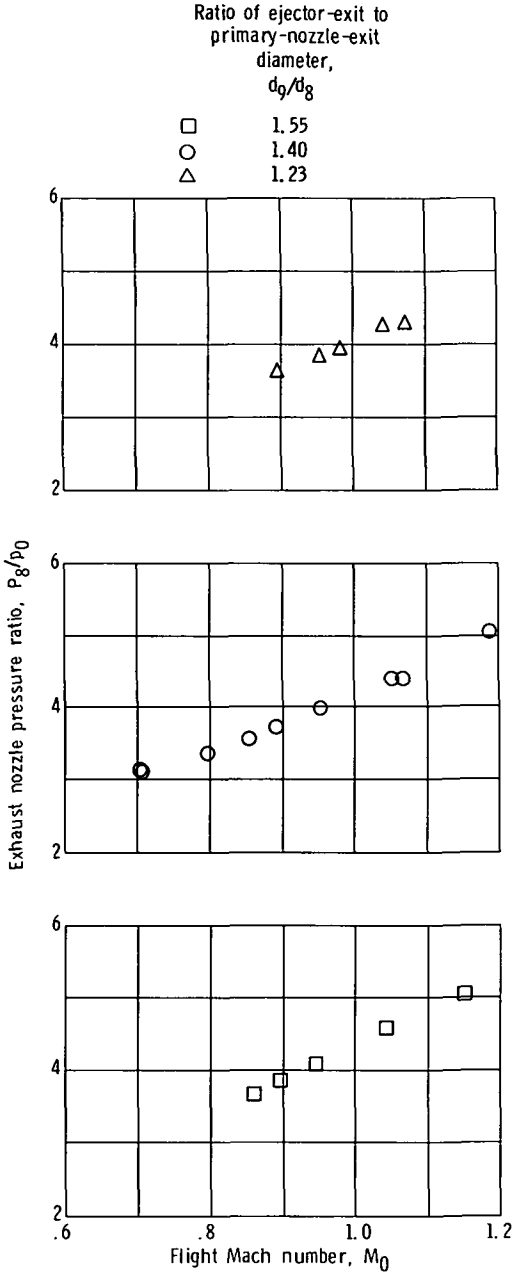

Figure 41. - Nozzle pressure ratio as function of Mach number for 10^0-20^0 doors.

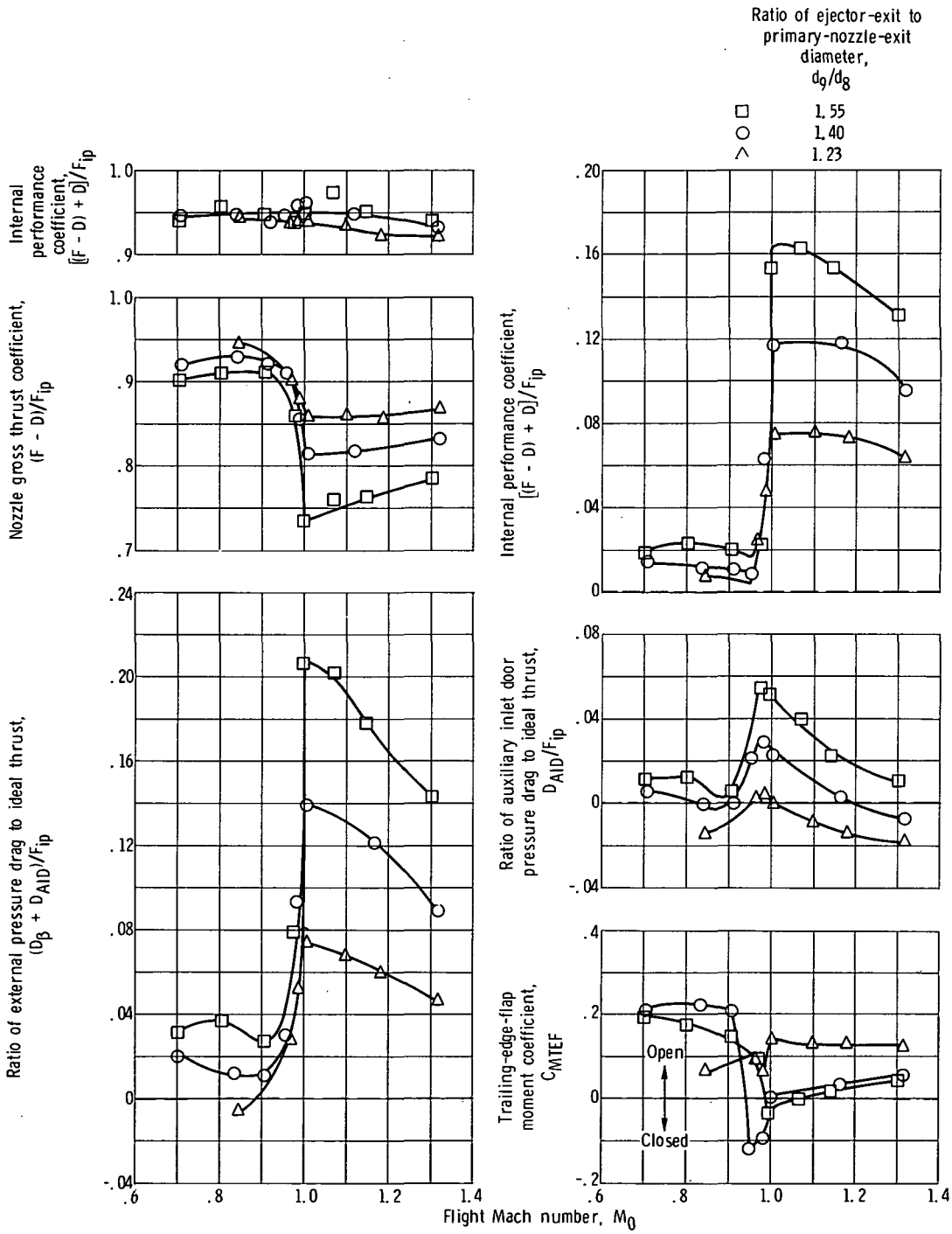

Figure 42. - Ejector nozzle performance characteristics as function of Mach number for 16° doors.

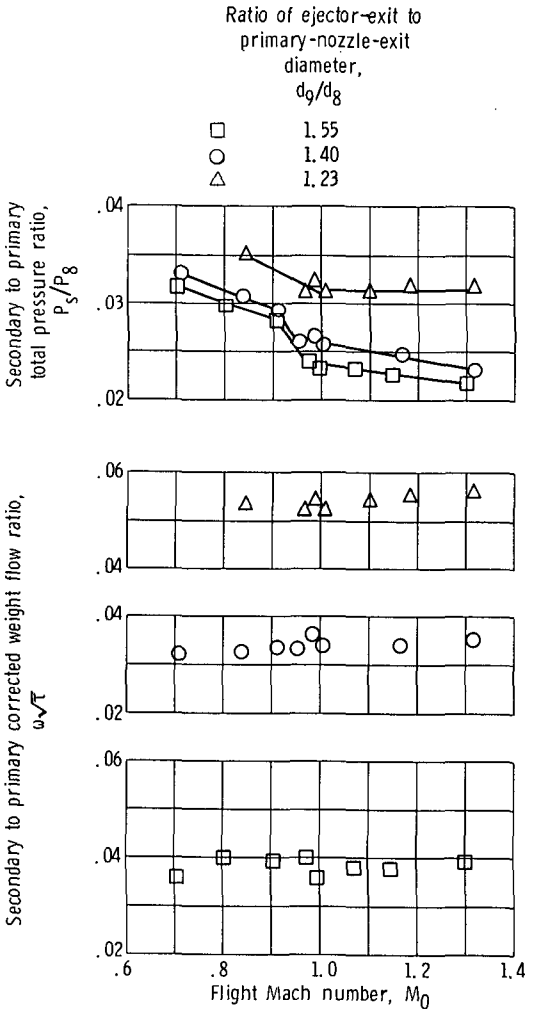

Figure 43. - Ejector nozzle pumping characteristics as function of Mach number for 16^0 doors.

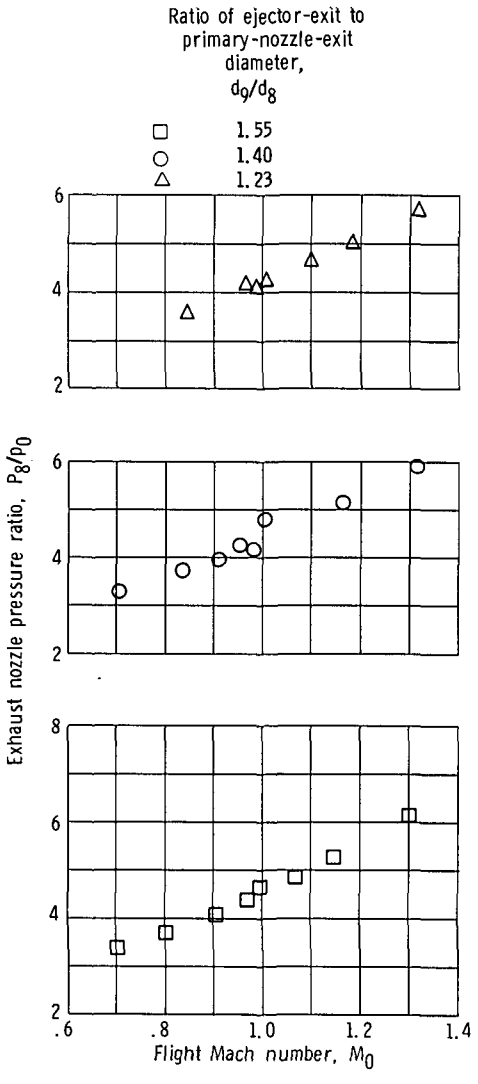

Figure 44. - Nozzle pressure ratio as function of Mach number for 16^0 doors.

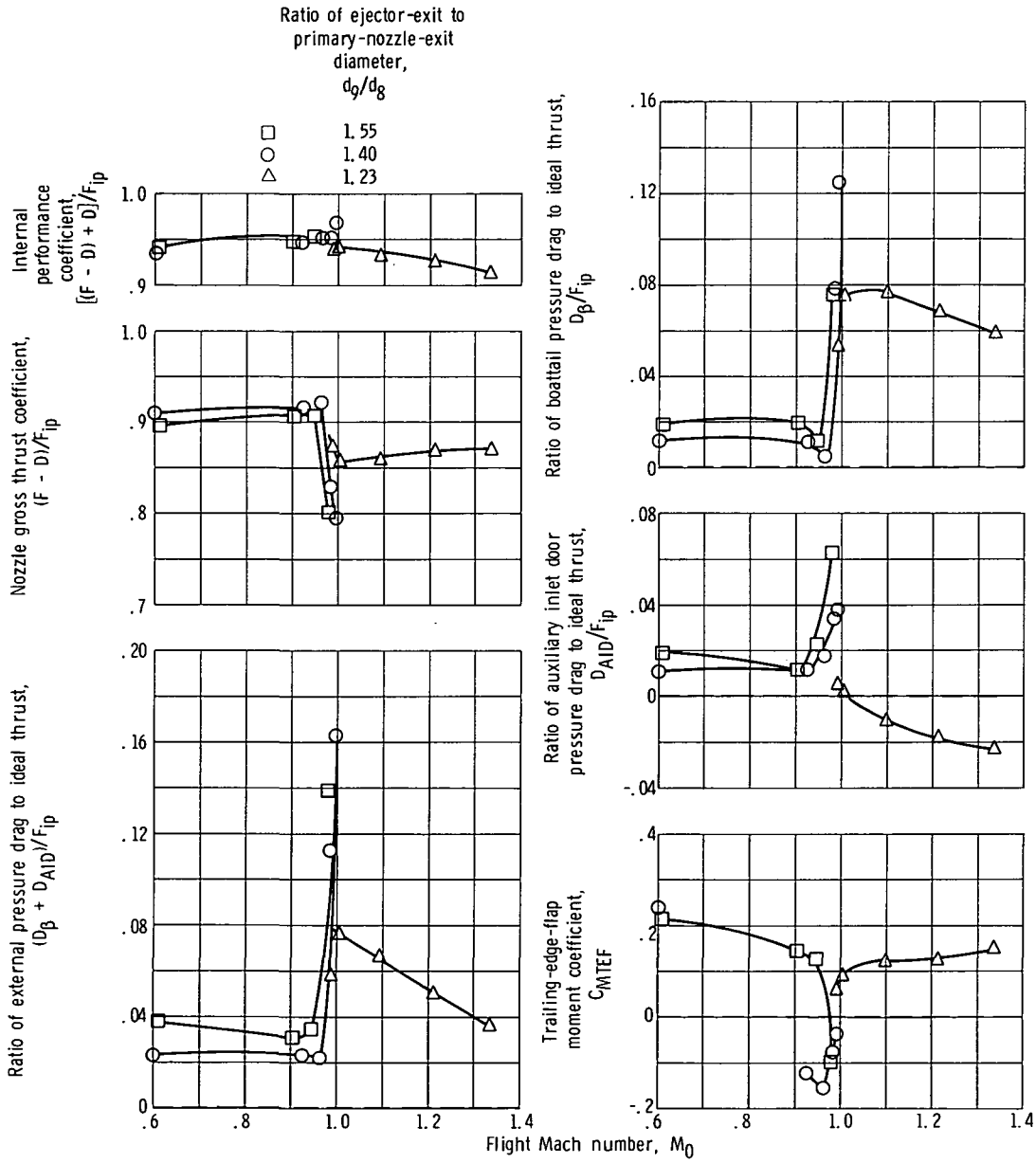

Figure 45. - Ejector nozzle performance characteristics as function of Mach number for 20^0 doors.

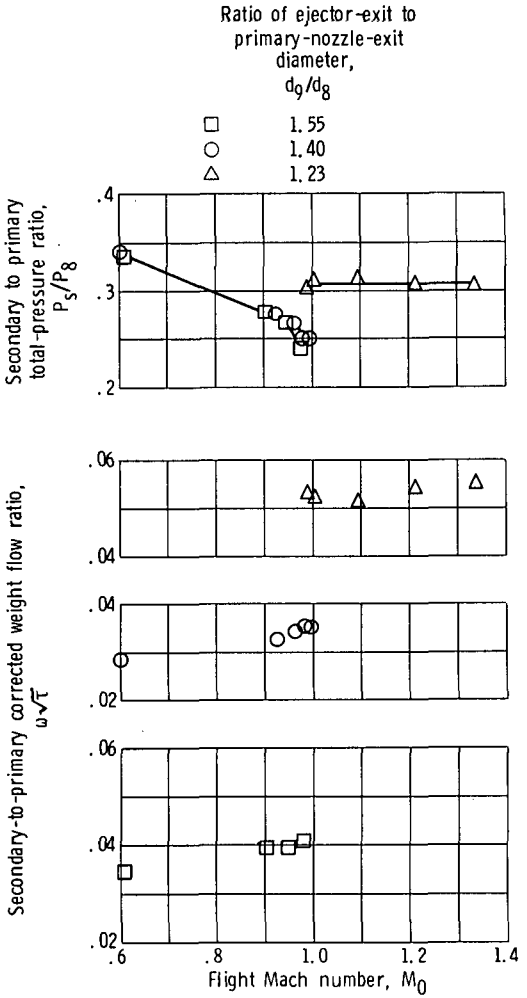

Figure 46. - Ejector nozzle pumping characteristics as function of Mach number for 20^0.

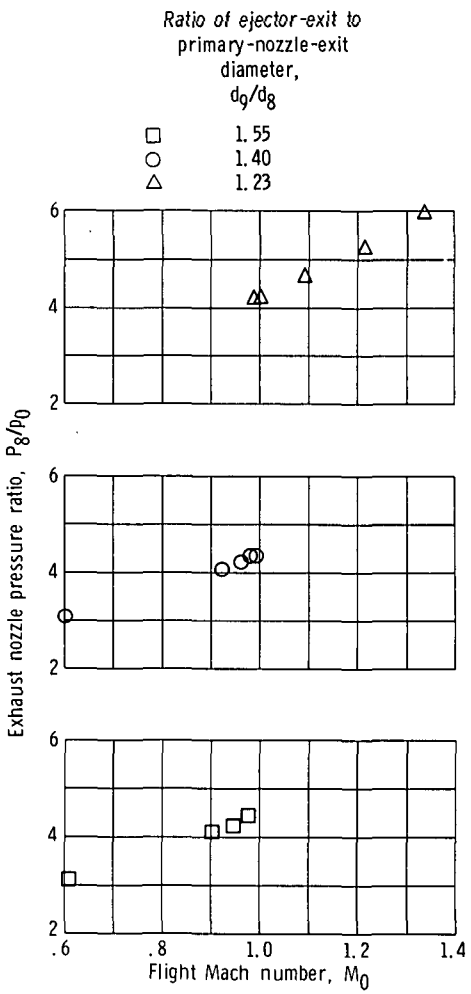

Figure 47. - Nozzle pressure ratio as function of Mach number for 20^0 doors.

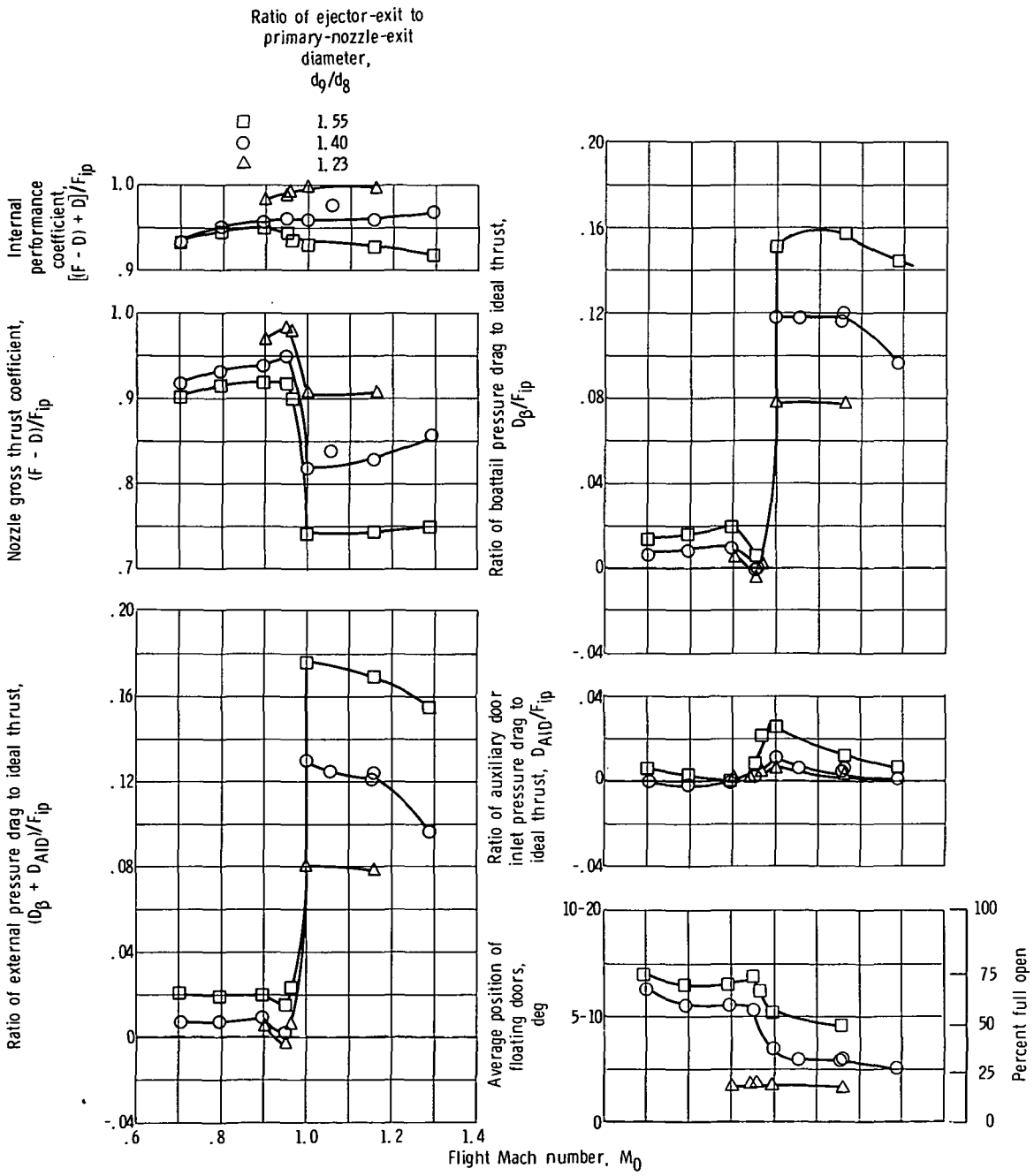

Figure 48. - Ejector nozzle performance characteristics as function of Mach number for unsynchronized floating doors.

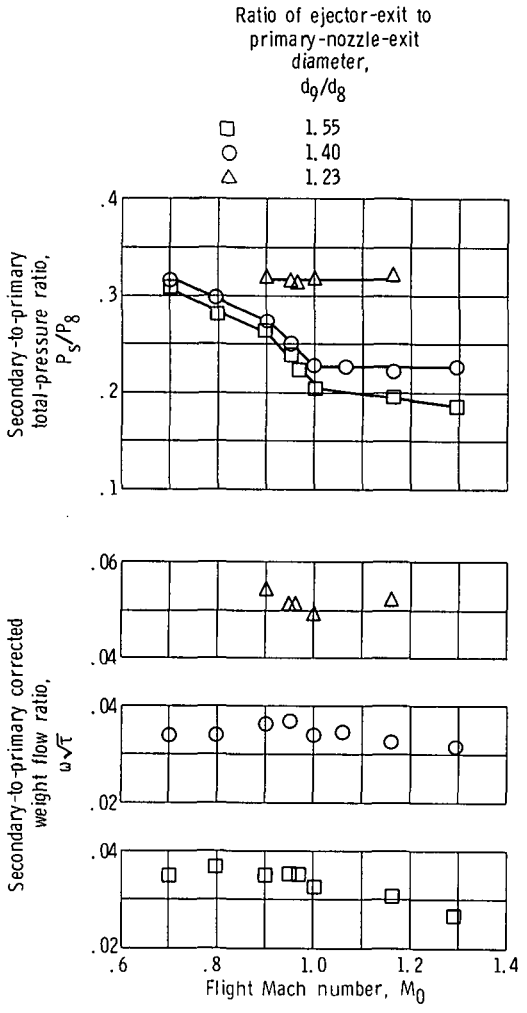

Figure 49. - Ejector nozzle pumping characteristics as function of Mach number for unsynchronized floating doors.

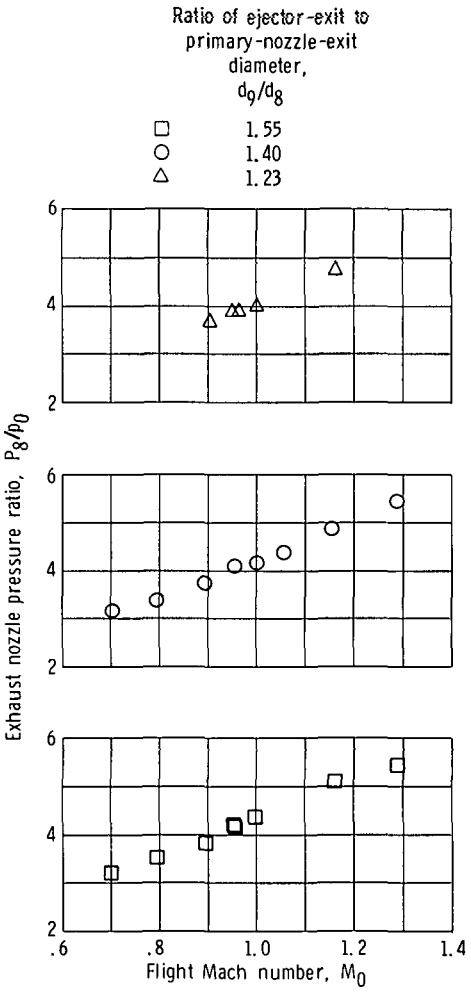

Figure 50. - Nozzle pressure ratio as function of Mach number for unsynchronized floating doors.

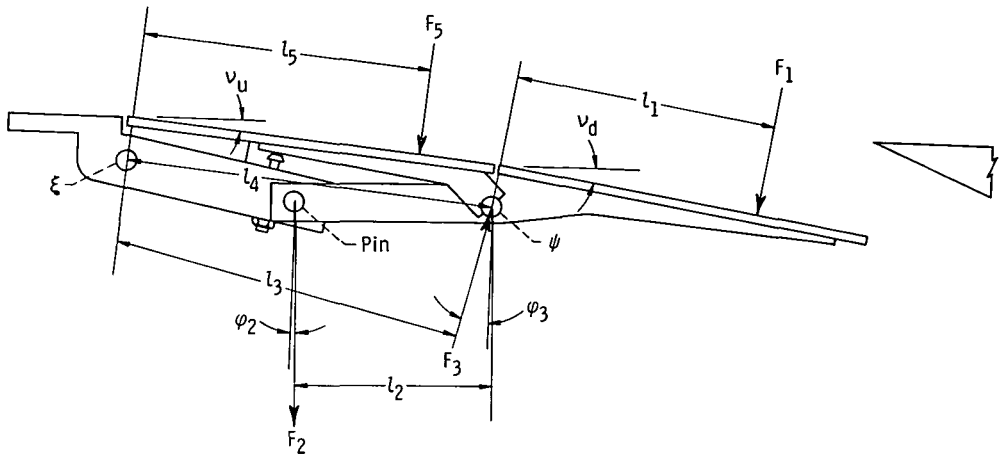

Figure 51. - Floating door moment analysis.

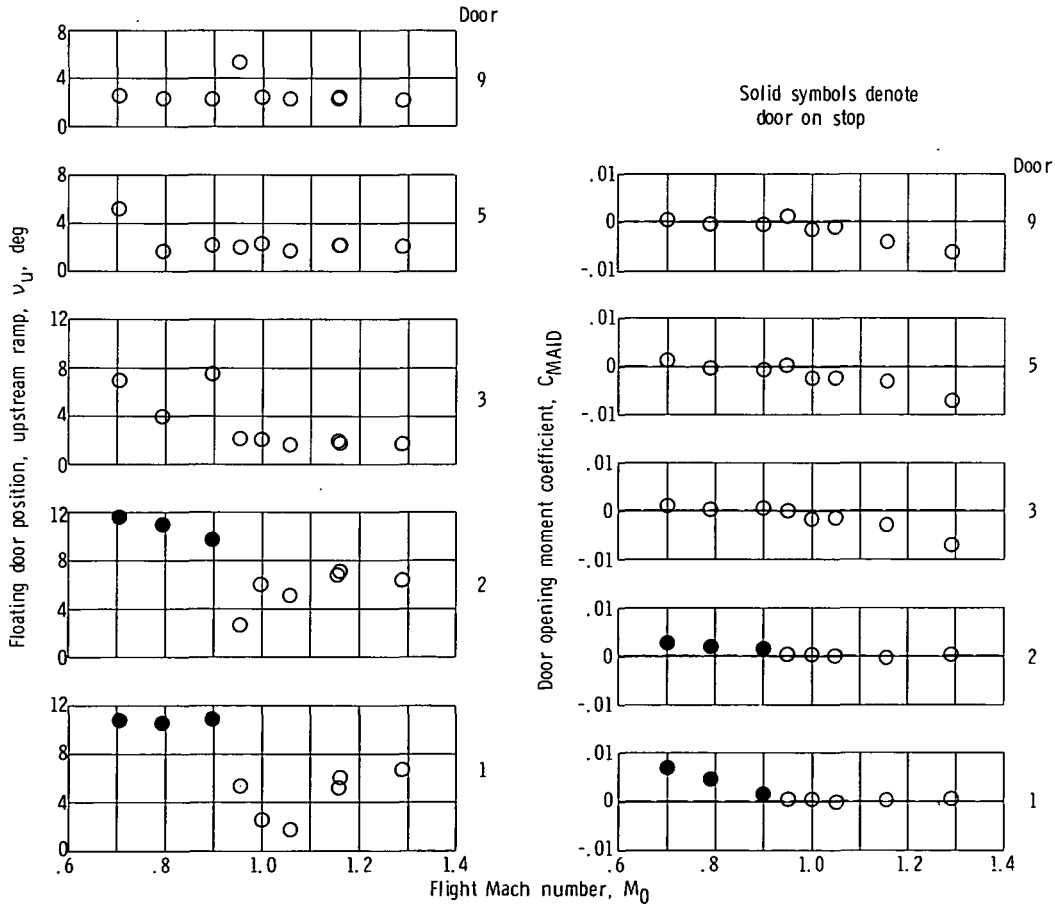

Figure 52. - Floating door position and moment coefficient as function of Mach number. Conditions: $d_9/d_8 = 1.40$ (minimum afterburning); $(\omega\sqrt{\theta})_s = 0.035$.

"The aeronautical and space activities of the United States shall be conducted so as to contribute . . . to the expansion of human knowledge of phenomena in the atmosphere and space. The Administration shall provide for the widest practicable and appropriate dissemination of information concerning its activities and the results thereof."

—NATIONAL AERONAUTICS AND SPACE ACT OF 1958

NASA SCIENTIFIC AND TECHNICAL PUBLICATIONS

TECHNICAL REPORTS: Scientific and technical information considered important, complete, and a lasting contribution to existing knowledge.

TECHNICAL NOTES: Information less broad in scope but nevertheless of importance as a contribution to existing knowledge.

TECHNICAL MEMORANDUMS: Information receiving limited distribution because of preliminary data, security classification, or other reasons.

CONTRACTOR REPORTS: Scientific and technical information generated under a NASA contract or grant and considered an important contribution to existing knowledge.

TECHNICAL TRANSLATIONS: Information published in a foreign language considered to merit NASA distribution in English.

SPECIAL PUBLICATIONS: Information derived from or of value to NASA activities. Publications include conference proceedings, monographs, data compilations, handbooks, sourcebooks, and special bibliographies.

TECHNOLOGY UTILIZATION PUBLICATIONS: Information on technology used by NASA that may be of particular interest in commercial and other non-aerospace applications. Publications include Tech Briefs, Technology Utilization Reports and Technology Surveys.

Details on the availability of these publications may be obtained from:

SCIENTIFIC AND TECHNICAL INFORMATION OFFICE

NATIONAL AERONAUTICS AND SPACE ADMINISTRATION

Washington, D.C. 20546